

ABSTRACT

Title of Document: Measurements of Soot Temperature in a Diffusion Flame Using a Digital Camera

Jose Castillo Moreno, Master of Science, 2012

Directed by: Peter B. Sunderland, Associate Professor,
Department of Fire Protection Engineering

Temperatures were measured in a laminar axisymmetric diffusion flame with a digital camera. The camera was a Nikon D700, modified to remove the Infra-Red (IR) cut filter and the anti-aliasing filter. Temperatures were obtained using ratio pyrometry at 550, 650, and 900 nm following deconvolution. The camera was calibrated with a blackbody furnace. Measurements were made for an 88 mm high laminar ethylene/air diffusion flame in co-flow on a burner with an 11.1 mm inside diameter. Soot temperatures were measured in the range of 1250 – 2000 K with an estimated uncertainty of ± 60 K. The diagnostic requires axisymmetric, optically thin flames, and regions with temperatures greater than 1250 K and soot volume fractions greater than 0.1 ppm. The results agreed with published measurements for this flame. The new diagnostics provide a convenient and economical way to perform these measurements with good accuracy and spatial resolution.

MEASUREMENT OF SOOT TEMPERATURE IN A DIFFUSION FLAME USING A
DIGITAL CAMERA

By Jose Castillo Moreno

Thesis submitted to the Faculty of the Graduate School of the
University of Maryland, College Park, in partial fulfillment
of the requirements for the degree of
Master of Science
2012

Advisory Committee:

Associate Professor: Peter B. Sunderland, Chair

Associate Professor: Andre W. Marshall

Associate Professor: Arnaud Trouvé

© Copyright by
Jose Castillo Moreno
2012

Dedication
To my parents

Acknowledgments

The author gratefully acknowledges the National Science Foundation (NSF) for its research support and David Urban for the equipment he provided.

This work has also been supported, in part, by the *Fulbright* program under the Panama Bureau of Educational and Cultural Affairs.

Special gratitude is due my parents and relatives for their loving support and providing me with an opportunity to study in the United States of America.

Thank you all for your constant encouragement and support.

Table of Contents

Dedication	ii
Acknowledgments.....	iii
Table of Contents	iv
List of Figures	v
Nomenclature	vii
Chapter 1: Introduction	1
Chapter 2: Experimental Methodology.....	6
Chapter 3: Results and Discussions	35
Chapter 4: Conclusions	44
References.....	46

List of Figures

Fig. 2.1	Ethylene flame. The height of the flame is about 88 mm from the top of the burner to the luminous tip of the flame	6
Fig. 2.2	Rotameters and needle valves.....	7
Fig. 2.3	Co-flow burner aligned with the camera.	8
Fig. 2.4	Scheme of the Santoro burner and radiation from the flame.....	9
Fig. 2.5	Co-flow burner burning an ethylene flame.....	10
Fig. 2.6	The Blackbody model (Oriol: 67032).....	11
Fig. 2.7	Matlab Program used to perform the integrations using Fig. 2.9, 2.10, 2.11	13
Fig. 2.8	Filter Transmittance vs. wavelength for the 550 nm.	14
Fig. 2.9	Filter Transmittance vs. wavelength for the 650 nm	15
Fig. 2.10	Filter Transmittance vs. wavelength for the 900 nm	15
Fig. 2.11	Camera automatic control mode using live view option.	16
Fig. 2.12	Spectral response for D700 camera	17
Fig. 2.13	Planck's curve for the blackbody using the calibrated temperatures.....	18
Fig. 2.14	Planck's curve for the blackbody showing the filter wavelengths	19
Fig. 2.15	Planck's curve for soot using the emissivity as a function of wavelength	19
Fig. 2.16	Planck's curve for soot showing the filter wavelengths	20
Fig. 2.17	Blackbody cavity image	23

Fig. 2.18	Gray scale/shutter time versus light intensity for 550nm	24
Fig. 2.19	Gray scale/shutter time versus light intensity for 650nm	24
Fig. 2.20	Gray scale/shutter time versus light intensity for 900nm	25
Fig. 2.21	Signal ratio vs. Soot Temperature.....	27
Fig. 2.22	Flame images using three band-pass filters.....	30
Fig. 2.23	Relationship between the Grayscale and size of the flame.	31
Fig. 2.24	Ruler used to find the position of the flame height.	32
Fig. 2.25	Abel filters options in Spotlight.....	33
Fig. 2.26	Abel deconvolved intensity for a 650 nm wavelength.	34
Fig. 3.1	Deconvolved intensity vs. radius at 7 mm flame height.....	35
Fig. 3.2	Deconvolved intensity vs. radius at 10 mm flame height.....	36
Fig. 3.3	Deconvolved intensity vs. radius at 15 mm flame height.....	36
Fig. 3.4	Deconvolved intensity vs. radius at 20 mm flame height.....	37
Fig. 3.5	Deconvolved intensity vs. radius at 50 mm flame height.....	38
Fig. 3.6	Deconvolved intensity vs. radius at 70 mm flame height.....	39
Fig. 3.7	Measured temperatures at three flame heights (15, 50 and 70 mm) above the burner and compared with soot volume fraction from Santoro's paper.....	40
Fig. 3.8	Measured temperatures at three heights above the co flow burner	41
Fig. 3.9	Measured temperatures at six heights above the co flow burner.....	42

Nomenclature

c = the speed of light [m/s].

f = the efficiency of the band pass filter.

F = is the spatial distribution of the physical property.

G_s = Grayscale

h = Plank's constant [6.626068×10^{-34} m² kg / s].

k = the Boltzmann constant [$1.3806503 \times 10^{-23}$ m² kg s⁻² K⁻¹].

n_{ab} = the calibration constant that couples the measured signal and the light intensity.

p = is the input data for the Abel transform.

r = radial distance.

S = the measured signal.

Greek Symbols

λ = Wavelength.

ε = Emissivity.

τ = the shutter time.

Subscripts

a = wavelength a.

b = wavelength b.

Chapter 1: Introduction

Soot is frequently present in flames giving the flame its typical orange or yellow appearance. Depending on the fuel type and the amount of substance that is present in the system, soot properties will be important in determining the soot temperature. Soot also contributes to radiant heat losses from flames, with peak emission at wavelengths in the infrared region of the spectrum.

A diffusion flame is a flame where the fuel and the oxidizer mix by diffusion. Diffusion flames generally yield more soot than premixed flames. The color of a laminar diffusion flame depends on the amount of soot in the flame. This is related to the oxygen supply and whether the fuel-oxygen is premixed. This ultimately determines the rate of combustion and thus, the different colors the flame has. If a typical Bunsen burner is analyzed, it burns with an incandescent yellow flame [1], primarily due to the generation of soot in the flame. The soot emits radiation. With the increase in oxygen supply, less radiation will come from the soot due to a more complete combustion [2]. In the colder part of a diffusion flame, the flame will have a reddish appearance transitioning to orange and yellow as the temperature increases [1]. When analyzing a flame temperature, there are many factors affecting the temperature. The blackbody radiation is only one part of the reason the flame has a characteristic color. There are other reasons such as the type of fuel being burned [1].

At room temperature, the blackbody appears black. This is mainly because the infra-red light cannot be perceived by the human eye. As the temperature is increased, the cavity in the blackbody will glow with an increase in the intensity and color. A perfect blackbody will have an emissivity equal to 1. However, in reality the blackbody will have an emissivity greater than 0.95

but less than 1. Nevertheless, this is a good approximation of a black material [3]. The radiation from the blackbody has a wavelength that depends only on the body's temperature [3]. This spectral intensity is called Planck's law. With the increase in temperature, the spectrum peaks at different wavelengths. At room temperature, most of the emission is in the infrared region [3]. If Planck's equation is plotted, the radiation is strongest at peaks that are given by Wien's displacement law. Therefore, as the temperature increases the glow color changes from red to yellow to blue.

Accurate measurements of temperature in a flame are essential for gaining fundamental insight into combustion processes. During the last decades, many combustion diagnostic methods, especially non-intrusive ones, have been developed to explore the soot properties in flames. Soot is present in most non-premixed, hydrocarbon/air flames where it affects flame reaction mechanisms and structure. Soot processes must be understood in order to achieve effective methods of computational combustion and predictions of flame radiation and pollutant emissions.

The radiative emission of soot particles in an ethylene/air flame is dependent on two quantities: the temperature and the soot volume fraction [4,5]. The use of a band-pass filter takes into consideration the temperature sensitivity under different configurations for soot, using ethylene as fuel. The filters isolate a band of wavelengths by providing a band of high transmissivity that results in a linear relation between the measured signal and the light intensity.

An ethylene diffusion flame in a co-flow has been studied in the past by Santoro [4,5]. In his work, the soot temperature was found using thermocouples. Santoro found that soot temperatures measured with a thermocouples peak at radial distances beyond where soot is at its highest concentration.

Gulder and co-workers [6,7] measured the soot temperature by spectral soot emission (SSE), in which line-of-sight radiation emission from soot is measured along chords through the flame. Many others used different techniques for temperature measurements [8-11]. Multi-wavelength, optical pyrometry is a common measurement technique to obtain the surface temperature of soot particles [12-18].

Long and co-workers [19, 20] used low-cost, consumer color digital cameras as a three-color optical pyrometer to measure the soot temperature within an axisymmetric flame. The uncertainty in the measured central wavelengths was estimated to be 5 nm, which corresponded to a shift of about 70 K in the calculated temperature [19]. Utilizing relatively low-cost but high resolution digital cameras as light detectors offers a tool to measure flame temperatures. In Long's work, the spectral response was characterized, which allowed for the creation of look up tables relating the three color ratios from the detector's RGB filters to the temperature of the soot. Long and co-workers also used a different digital camera. The blackbody calibration in Long's work was done using a temperature range from 800 to 1200 °C in increments of 50 °C.

S. di Stasio and P. Massoli [21] measured the soot temperature by two-color pyrometry. In their work, the calculations were carried out taking into account particle shape, different expressions for monochromatic emissivity, optical property variations and a finite light-detection bandwidth.

T. Panagiotou and Y. Levendis [15] used a three-color, near-infrared, optical pyrometry method with wavelengths centered at 998, 810, and 640 nm. In their work, flames were assumed to be optically thin. Their experiments suggest agreement among the three individual temperatures obtained from three-color pyrometry.

Spotlight is a cross-platform GUI-based software package designed to perform image analysis. These images are measured with the interactive mode found in Spotlight. Image processing operations can be employed to enhance an image before various statistical and measurement operations are performed meaning that the image can be rotated and aligned with other images for better analysis. The objects can be analyzed simultaneously with independent areas of interest. Spotlight saves results in a text file that can be imported into other programs for further analysis. This software can be run on a Microsoft Windows platform. [22]

Field measurement of soot temperature within a steady laminar, ethylene/air diffusion flame using a consumer single-lens reflex (SLR) camera with two-ratio pyrometry was established in this research. The main objective was to convert the intensity of a grayscale form of a image to a temperature value. Grayscale in this paper is the result of measuring the intensity of light at each pixel in a single band, electromagnetic spectrum converted from a full color image to grayscale.

A key part in the ratio pyrometry method is that it requires a pair-wise combination using band-pass filters. A band-pass filter is a device that allows wavelengths within a certain range to pass. In other words, it attenuates wavelengths outside this range. An ideal bandpass filter would have a flat passband and would, therefore, attenuate all frequencies outside the passband. In reality, no bandpass filter is ideal. The bandwidth of a filter is the difference between the upper and lower cut-off frequencies. Another important term in this research is the full width at half maximum (FWHM), which corresponds to a difference between the two extreme values equal to half of the maximum values of the filter wavelengths. This value is widely used in signal processing to define the bandwidth, and it was used in the filters used in this research. [23]

The soot temperature results obtained in this paper are compared with those from Santoro and co-workers [4,5] providing reasonable results.

The objectives of this work are:

1. Explore full-field measurement of soot temperatures using ratio pyrometry with a digital camera
2. Improve field measurements of soot temperature from previous methods.

Chapter 2: Experimental Methodology

A steady laminar ethylene/air diffusion flame was generated using a co-flow burner Fig. 2.1, which is a replica of that used by Ref. [4]. It consists of two concentric tubes of 11.1 and 101.6 mm inner diameters. Glass beads and ceramic honeycomb were used in the coflow. The fuel tube extends 4 mm beyond the exit plane of the air honeycomb. The ethylene flow rate was maintained at 4.35 mg/s while the air flow was 856 mg/s through needle valves. The burner assembly was mounted on a table base, which provided for three dimensional positioning capabilities. Radial traversing of the burner was accomplished using a manual translation stage, which was mounted on the table base.

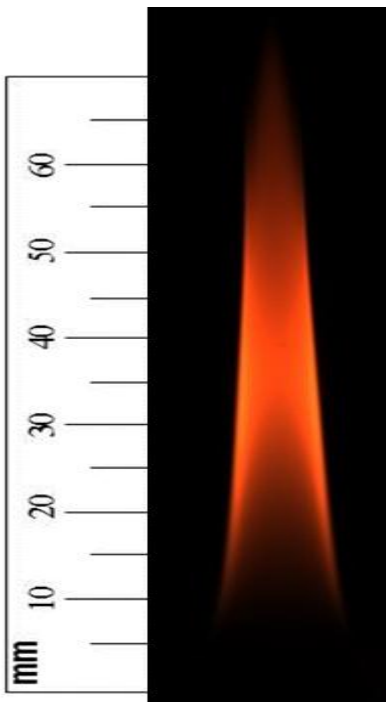


Fig. 2.1 Ethylene flame. The height of the flame is 88 mm from the top of the burner to the luminous tip of the flame.

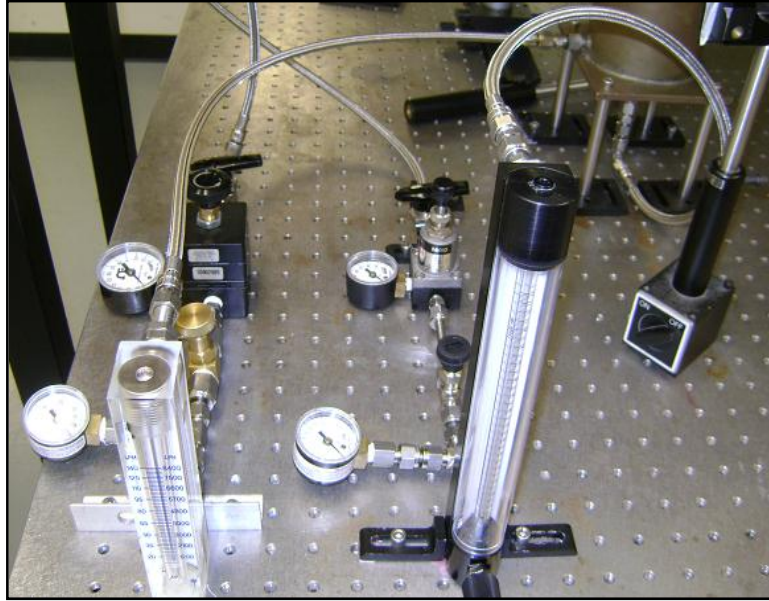


Fig. 2.2 Rotameters and needle valves.

Rotameters were used to measure the air and fuel flow rates and were calibrated using soap bubble meters as seen in Fig. 2.2 and 2.3. Once calibrated, it was necessary to test the values of air and fuel flow. Therefore, an 88 mm flame height was set using the calibrated values. This showed that the calibration can be accurately used in the experiments. An important property of the rotameter is the ability to show changes in either fuel or air concentration. This can be used to investigate the relative importance of different fuel flow rates to estimate the effect of changes in flame height and width.



Fig. 2.3 Co-flow burner aligned with the camera.

Flexible hoses were used to make the connections from the air and fuel rotameters to the Santoro burner. The fuel hose connection was made from the bottom of the burner, and the airflow was made from the side of the burner. The hoses and valves were fixed to the table along with the camera and the Santoro burner. This provided greater stability to the whole system. A black foam panel was set behind the burner to avoid any reflection from the flame and also to block any light from non-flame sources.

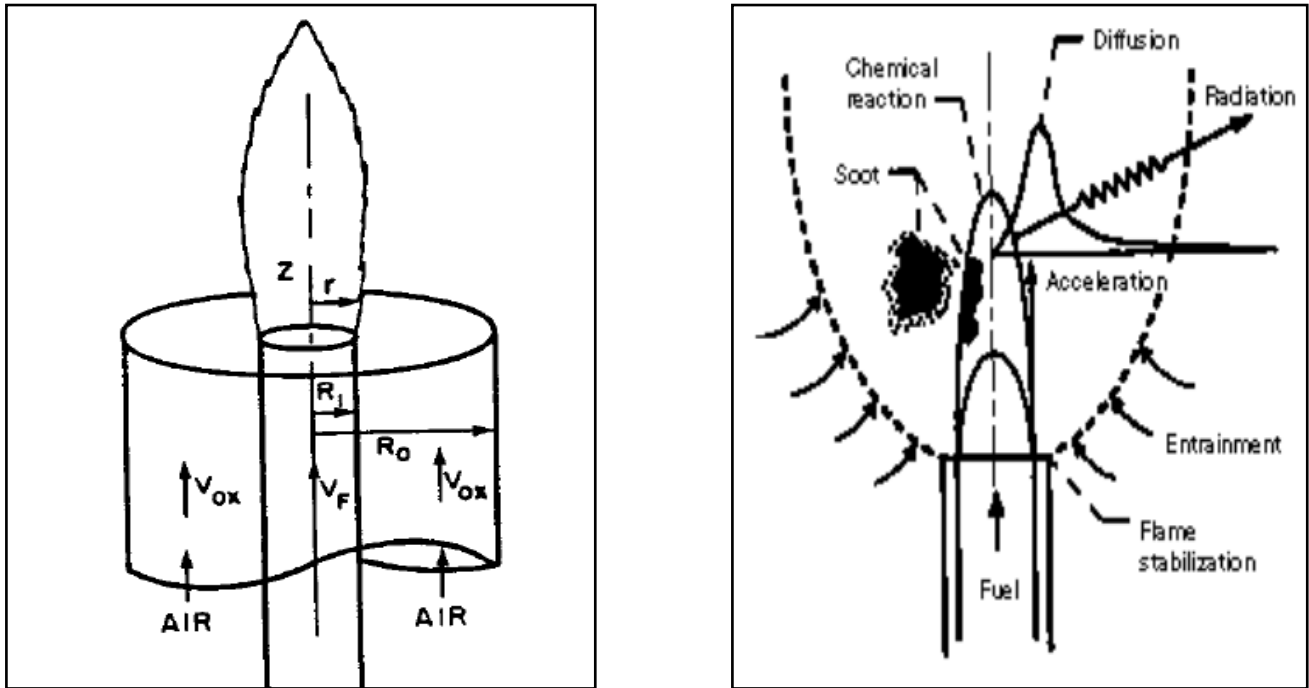


Fig. 2.4 Scheme of the Santoro burner and radiation from the flame.

The Santoro burner as seen in Fig. 2.4 is used to make the flame steady and axisymmetric. This is of utmost importance for the measurements. The oxidizer, air, comes from the bottom of the burner through a honeycomb, which reduces entrainment, and the fuel comes from a tube surrounded by the honeycomb. The oxygen and fuel diffuse into each other; where they meet, the flame occurs. Once a steady axisymmetric flame is obtained, it is possible to analyze the flame, focusing mainly on the radiation coming from the soot as seen on the right hand side of Fig. 2.4. The visible flame height was 88 mm for this non-sooting, ethylene flame as shown in Fig. 2.1. The flame was steady, optically thin and axisymmetric.

A Nikon D700 DSLR (digital single –lens reflex) camera with a 50 mm f/1.4 AF-D Nikkor lens was used for temperature measurements. See Fig. 2.5. The current price of the Nikon D700 is US \$3000, which is unusually low for a camera that can be used for quantitative scientific research. The D700 utilized a sensor (36.0×23.9 mm) with 12.1 million effective pixels (4256×2832). The lens was set to f/1.4. The camera was modified by removing the IR Cut Filter to expand the camera’s acceptable wavelength range to infrared light, which improves the soot temperature measurement accuracy. The camera was further modified by removing the anti-aliasing filter to eliminate the blurring process of high frequency signal. In addition, a clear filter was added to restore focus with an eyepiece.



Fig. 2.5 Co-flow burner burning an ethylene flame.

All image post-processing options were set to either “normal” or “none” to avoid built-in image processing algorithms. The ISO was set to 200. A white balance of direct sunlight was selected. Files were saved in an uncompressed format. Decoding of the Nikon-specific data format was done using dcrw [24]. It avoided gamma correction associated with most consumer software.

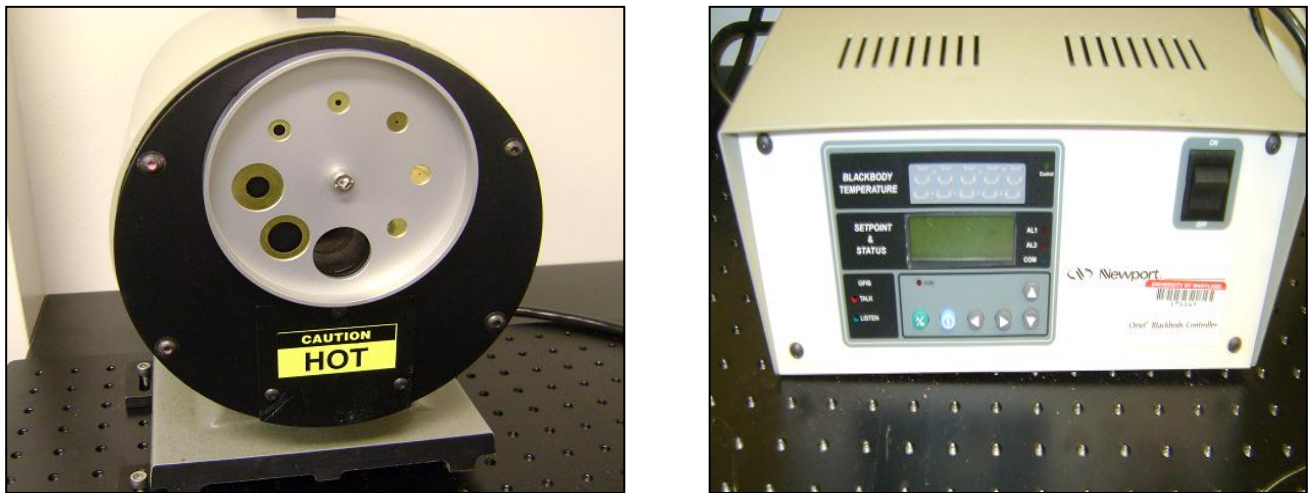


Fig. 2.6 The Blackbody model (Oriel: 67032) and a temperature limit of 1100 °C.

The linearity of camera signal response to light intensity was calibrated using a blackbody calibration source as seen in Fig. 2.6. The blackbody provided an accurate stable source of infrared radiation of known flux and spectral distribution, which resulted in a calibration against a standard value as seen in Fig. 2.17. The high surface emissivity and the geometrical form of its cavity produced an emissivity near unity. This source emits blackbody radiation by multiple reflection, absorption and re-emission of the thermal energy. The thermal energy of the cavity is provided by a ceramic sealed heater coil that uniformly heats the cavity cylinder to temperatures from 50 °C to 1100 °C.

The cross-platform GUI-based software Spotlight [22,25] was used to perform the analysis on sequence of images for the ethylene flame to obtain the grayscale value for a given filter wavelength. This software uses Abel deconvolution. This program is the simplest among those commonly used methods to obtain the real signal values of a flame. Spotlight supports a number of image processing operations, which can be used to enhance image details so that images may be analyzed more easily. A sequence of operations may be performed on a user-defined area of interest (AOI) to apply to each frame of a set of images. The 16-bit version of the Spotlight software was used.

Soot temperatures were measured with the aid of three band-pass filters (Maker: Newport, Models: 20BPF10-550, 20BPF10-650, 20BPF10-900) with central wavelengths at 550, 650 and 900 nm, respectively and with full width at half minimum (FWHM) of 10 nm. These filters were placed in front to the camera lens. These bandpass filters isolate a band of wavelengths from the total spectrum by providing a band of high transmission while rejecting the spectral energy on both the long and short wavelength sides of the transmission band.

As seen in Fig. 2.8, 2.9 and 2.10, each bandpass filter has a peak transmittance occurring at approximately 550, 650 and 900 respectively. These curves were converted into Matlab functions [26]. Using the fitted curve option in Matlab all points are analyzed and converted into a single mathematical expression that can be called along with other functions and integrated using a basic Matlab program as seen in Fig. 2.7.

```

function f = intval( x,T )
c1=1;
c2=1.439E-2;%Constants defined
x5=x.^-5;
xr=x.^-1;
den=(exp(c2.*xr.*(1/(T+273))))-1;
rden=den.^-1;%reciprocal of the Denominator
num=c1.*x5;
load curve650;
curve = curve650(x);
g=num.*rden;%Numerator
gg = g'.*curve;
f=trapz(x,gg)
end

```

Fig. 2.7 Matlab Program used to perform the integrations using Fig. 2.8, 2.9, 2.10

Images were converted to grayscale. First each pixel's red, green, and blue (RGB) values were obtained in the linear intensity encoding provided by spotlight. These values were then averaged in Spotlight by assigning a weight percentage, typically 30% for the red value, 59% for the green value, and 11% for the blue value, to each one of them. The resultant number is the desired linear intensity value; it typically needs to be gamma compressed to get back to a conventional grayscale representation. The conversion from RGB to grayscale reduces the number of data points in plots of intensity versus location. However, such conversion was favored here because this type of averaging reduces scatter, and it collapses the three color intensity profiles at each height into a single profile.

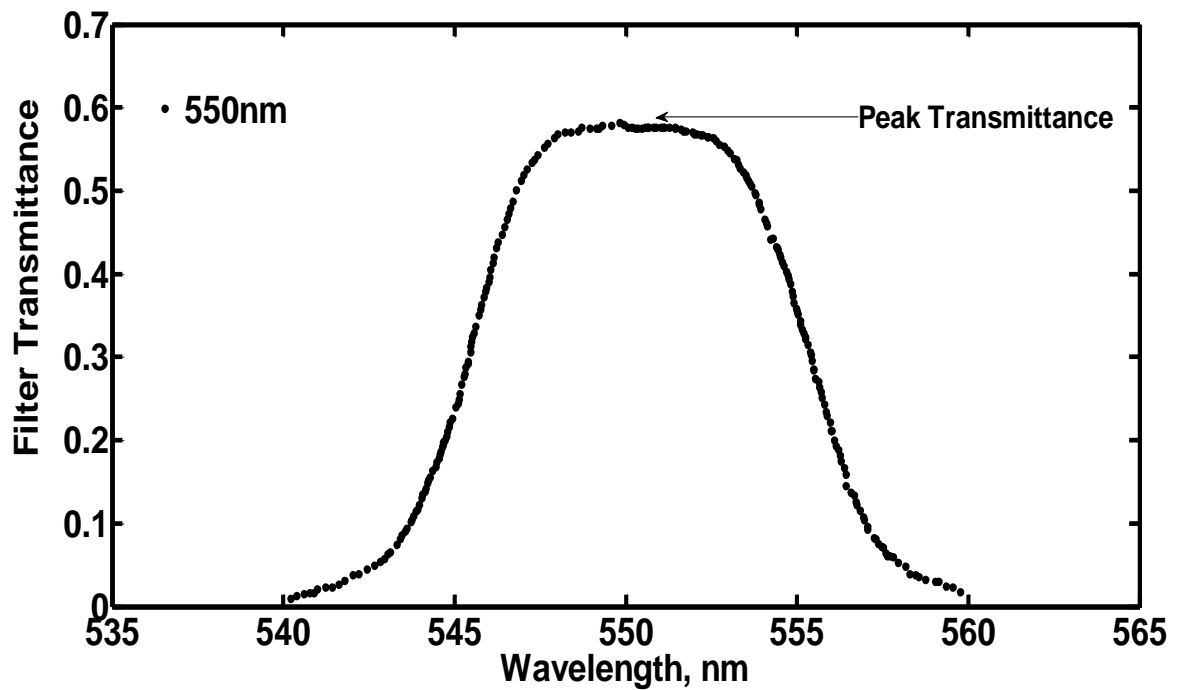


Fig. 2.8 Filter Transmittance versus wavelength for the 550 nm bandpass filter. [27]

Each filter provides a narrow range of transmittance around the specific wavelength with a peak transmittance around 60%. Depending on the wavelength for each filter, the filter will have a thin layer with a characteristic color. The other side of the filter will have a mirrored quality. The side with the color layer must be placed facing the flame. This is mainly due to avoid any loss in signal intensity by the photons reflecting off the mirror side. The intensity of radiation is, therefore, not lost and is captured by the camera.

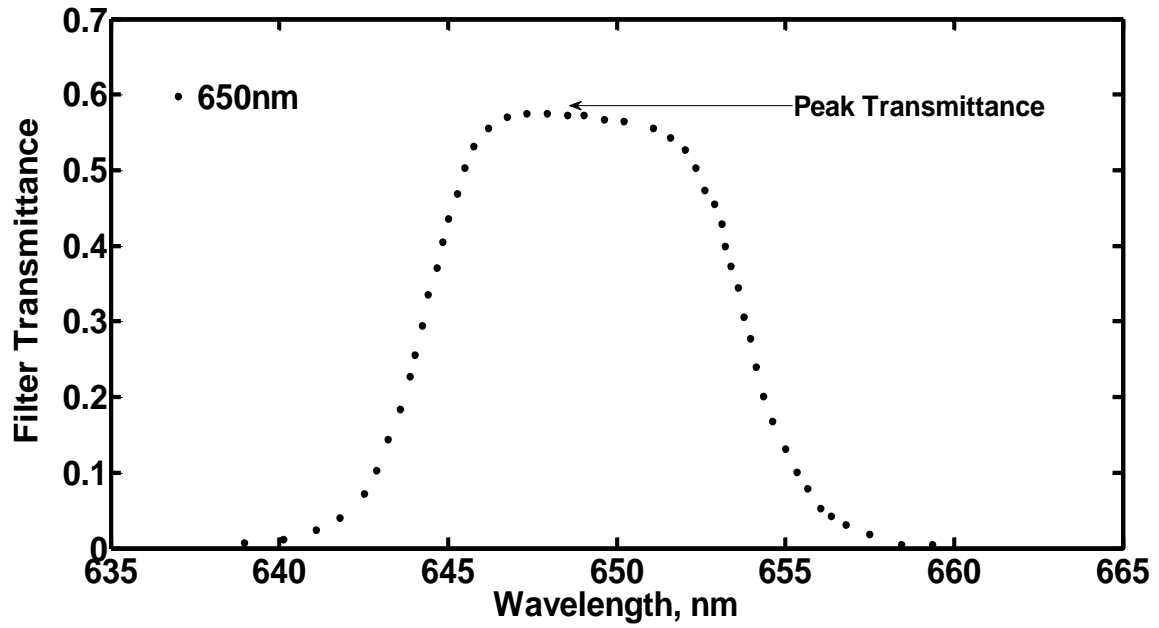


Fig. 2.9 Filter Transmittance vs. Wavelength for the 650 nm Bandpass Filter. [27]

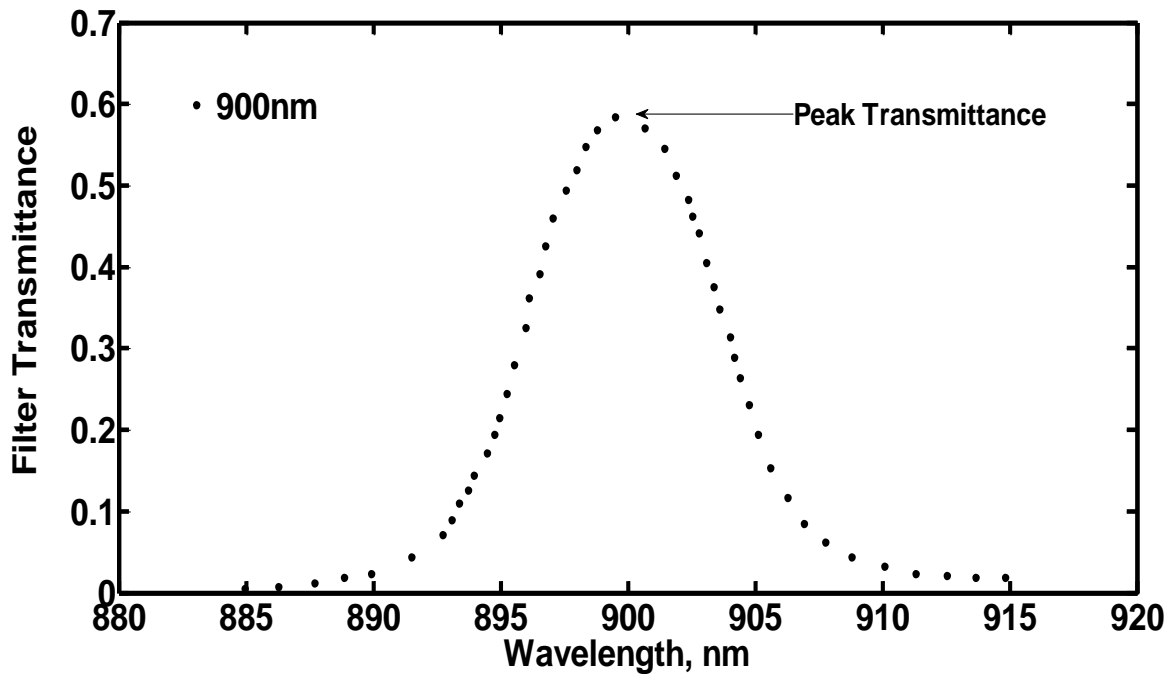


Fig. 2.10 Filter Transmittance vs. Wavelength for a 900 nm Bandpass Filter. [27]

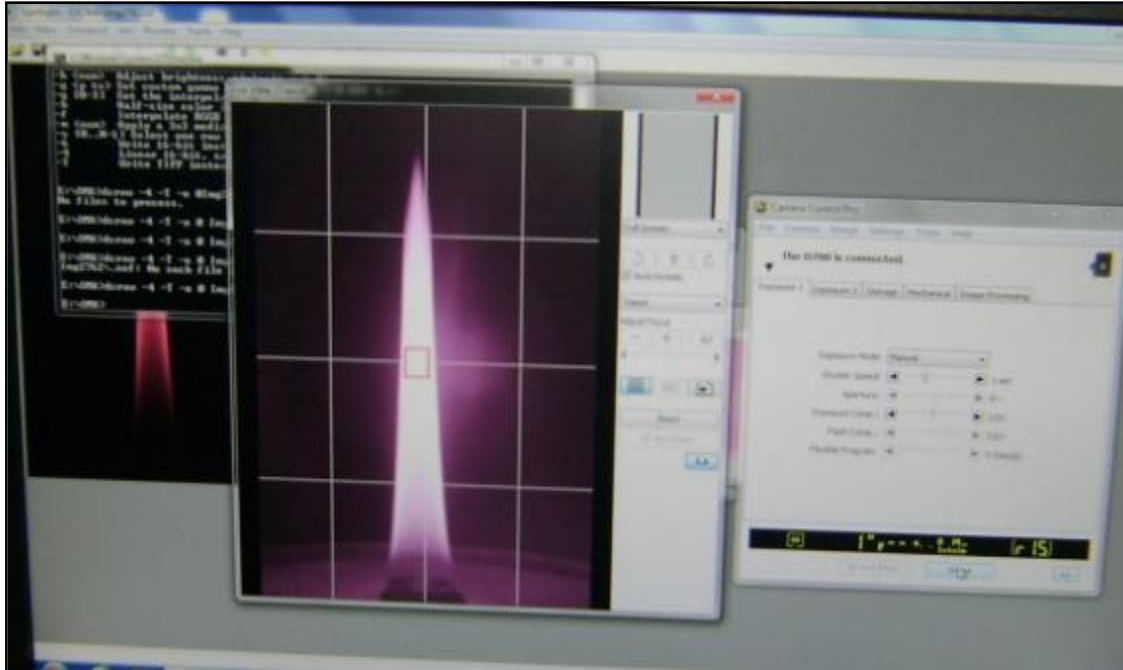


Fig. 2.11 Camera automatic control mode using live view option.

In terms of how lenses handle focusing, the manual focus and live view option in the D700 offers an increase in the level of precision when compared to automatic focus lens. Manual focus systems can generally achieve a very high number of "hits" in terms of the sharp images they produce. One problem, however, is that the filters are often not perfectly aligned with the cameras, and it only takes a minimal deviation of a millimeter to produce a visible focus error. The D700 camera enables a live image to be viewed on the display prior to taking the shot. It is usually possible to zoom into this view from a distance and still carry out focusing with great precision. Enhanced focusing screens, a well-aligned manual focus system and use of the Live View mode all help to make focusing more precise. As seen in Fig. 2.11 the camera live view option can be used along with Spotlight program to analyze the images with great accuracy and avoid image saturation or errors in the measurements.

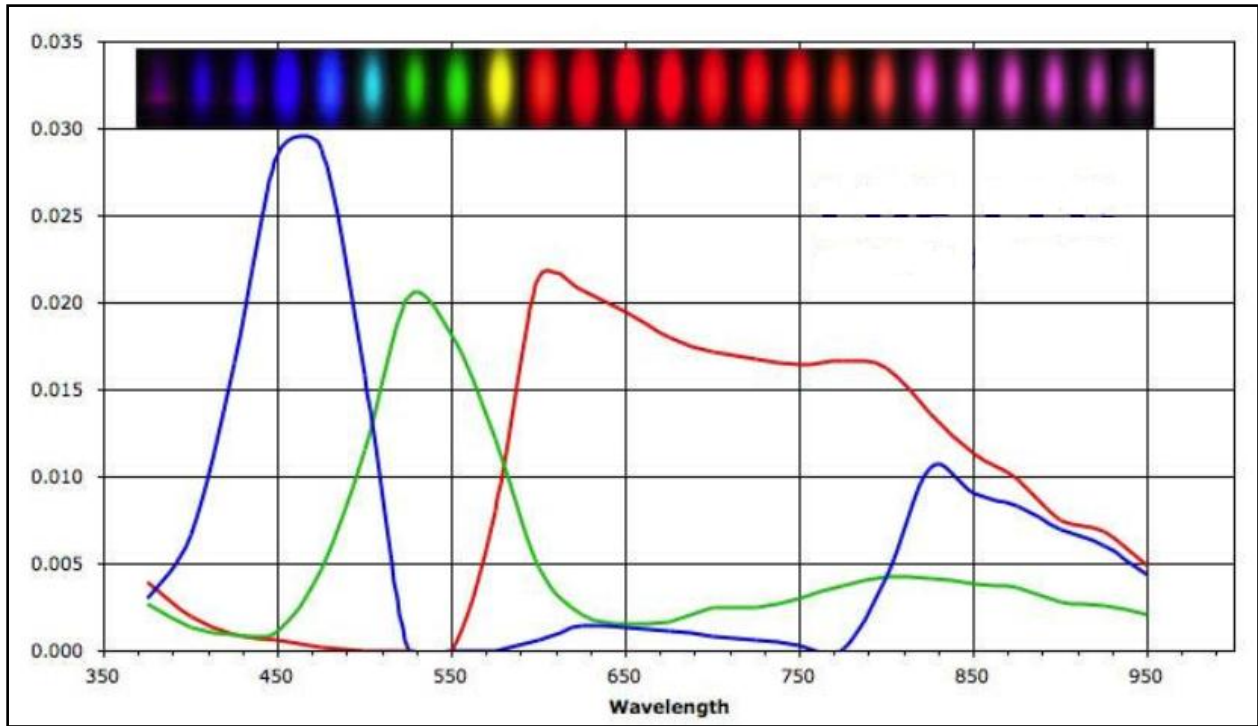


Fig. 2.12 Spectral response for D700 camera [28]

In order to more fully understand the spectral response of a DSLR camera, it is necessary to analyze the selected camera image sensors. Using Fig. 2.12 where the spectral sensitivity is shown, the response of a camera is seen under the visible and the infrared light, UV. The color dots at the top of the Adjust RGB Curves graph are actual images taken by a Nikon D700 at the corresponding wavelengths. These response curves are the spectral response after removing the infrared cut filter to expand the camera's acceptable wavelength range to include infrared light over 700nm. The filters were selected based on the spectral response of the camera enabling as much light as possible to be sensed by the camera sensor shown in Fig. 2.12.

An Oriol Blackbody source (Model: 67032, 25.4 mm cavity opening and a temperature limit of 1100 °C) were used to calibrate the camera. This calibration relates the measured signal and the intensity of radiation provided by Planck's law:

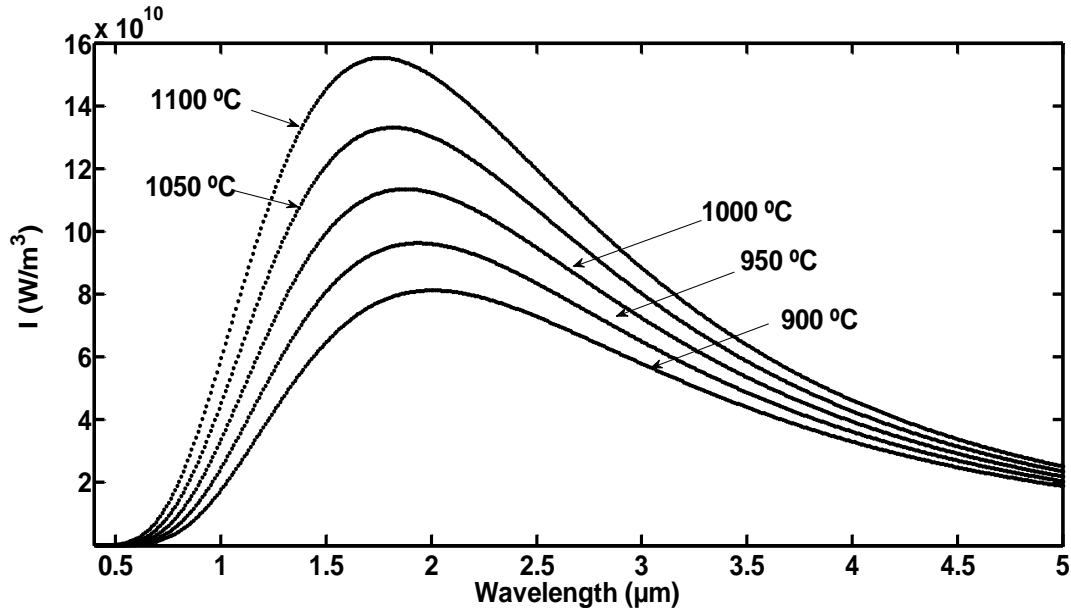


Fig. 2.13. Planck's curve for the blackbody using the calibrated temperatures.

The primary law governing blackbody radiation is the Planck Radiation Law, Eq. 2.1, which governs the intensity of radiation emitted per unit surface area into a fixed direction (solid angle) from the blackbody as a function of wavelength for a fixed temperature. Figure 2.13 shows Planck's curve plotted for the range of temperatures used in the calibration. Figure 2.14 shows the same curve but only the areas where the three filter wavelengths 550, 650 and 900 nm are used. As shown in Fig. 2.14 the camera has an acceptable sensitivity at these wavelengths.

$$I(\lambda, T) = \frac{2\pi hc^2 \varepsilon(\lambda)}{\lambda^5 (e^{hc/\lambda kT} - 1)} \quad 2.1$$

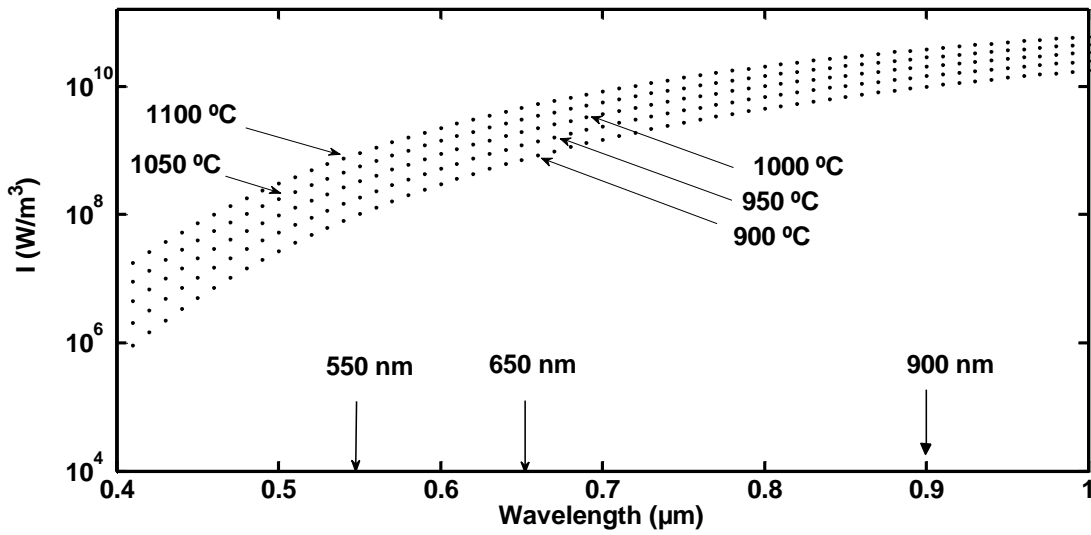


Fig. 2.14. Planck's curve for the blackbody showing the filter wavelengths.

Also plotted is the soot intensity of radiation as seen in Fig. 2.15 and 2.16. The emissivity is found using the result by Charalampopoulos [29] where emissivity changes to the wavelength is $\lambda^{-1.38}$

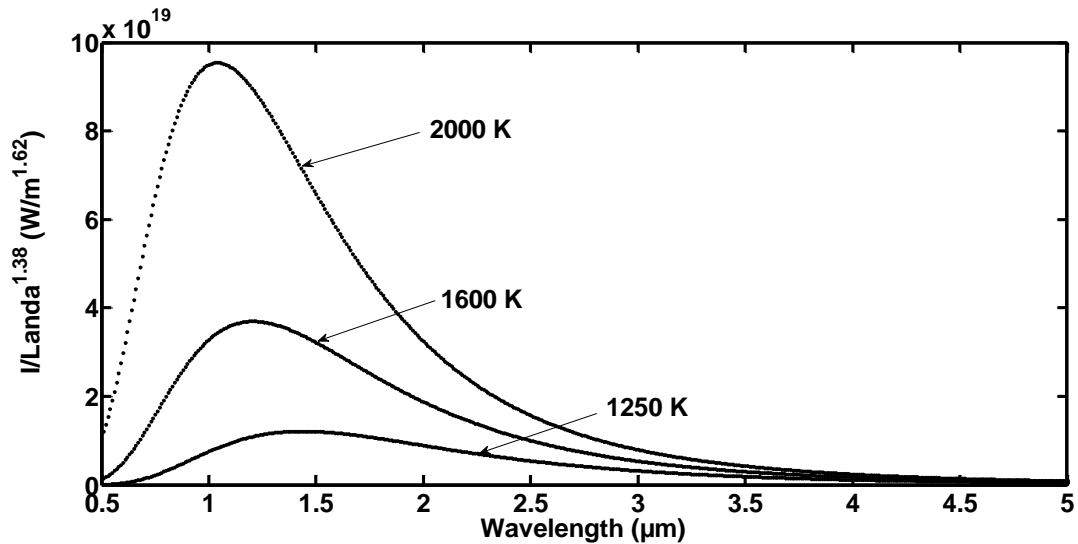


Fig. 2.15. Planck's curve for soot using the emissivity as a function of wavelength

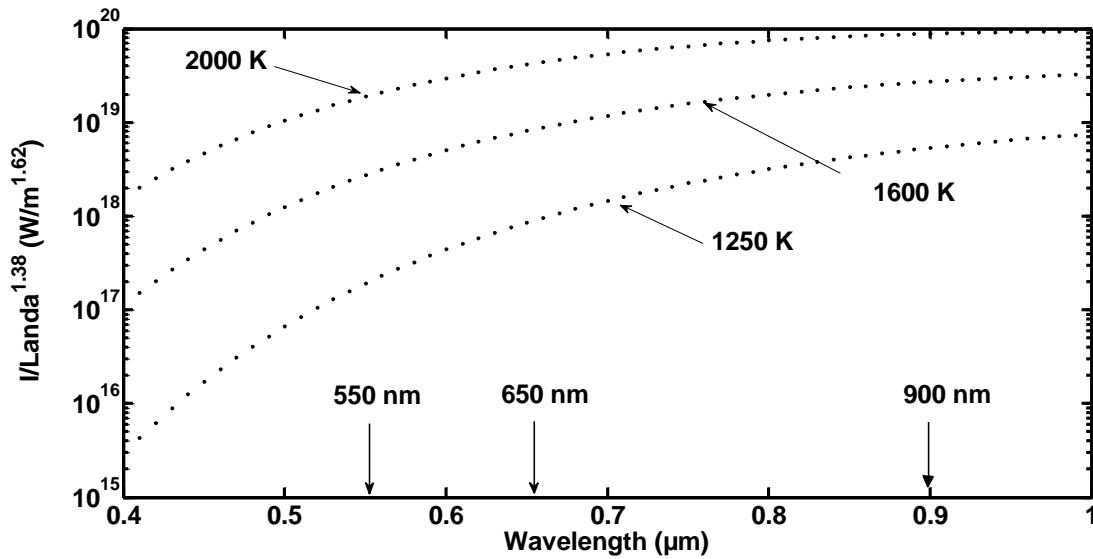


Fig. 2.16. Planck's curve for soot showing the filter wavelengths.

Figure 2.14 and 2.16 exhibit the same behavior. The filter wavelength are shown; 550, 650 and 900 nm. If both graphics are compared, it can be seen that the intensity using soot increases because of the higher temperature at which these figures are plotted. Since the emissivity for the blackbody is constant, and it is a number close to one, the intensity of radiation is not affected. However, for soot the emissivity changes accordingly to the wavelength. Moreover, since the wavelengths are values of the order of nanometers, the final result of changing the emissivity is a higher intensity than that expected for the blackbody. Since the exponent of the wavelength was raised to a power of - 1.4, the final result of the intensity was much higher. In Fig. 2.15 and 2.16 three temperatures were chosen to represent the whole range in which the soot temperatures were obtained.

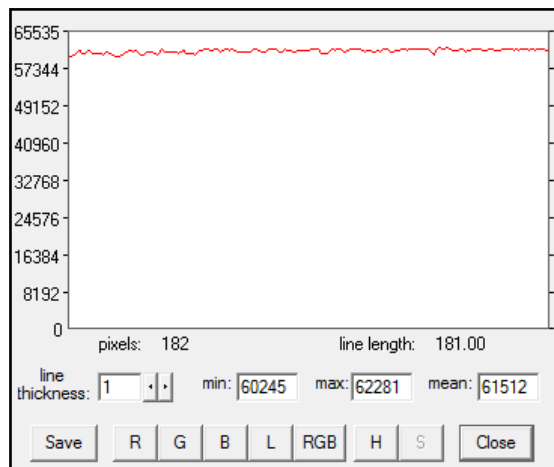
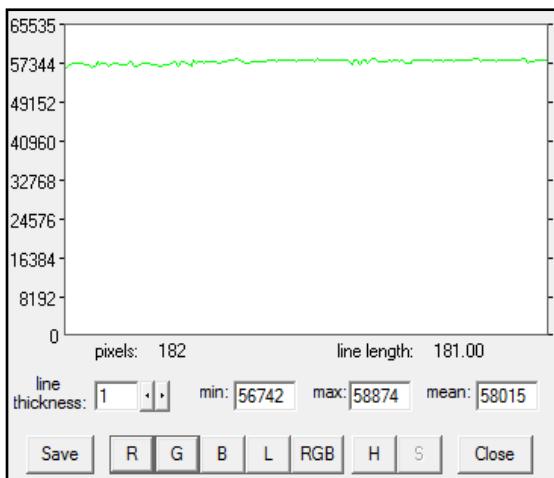
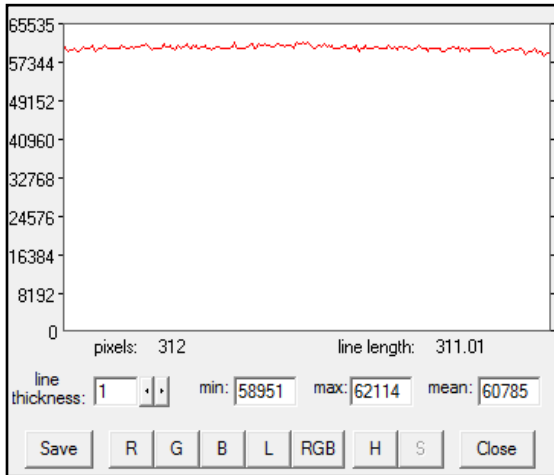
An optimal object distance of 13.5 cm was found to maximize the flame image in the frame such that the sensor could be fully used. The shutter trigger was controlled remotely to minimize vibrations. The D 700 recorded images of a blackbody source at temperatures ranging from 900 to 1100 °C, in 25 °C increments. As seen in Figs. 2.18, 2.19 and 2.20 the grayscale response varies linearly with the intensity of radiation. Therefore, a different temperature increment can be used rather than 25 °C. Thus, a 10 degree increment was also used, and no difference was found in the calibration results. Spotlight [22] was used to obtain the grayscale from each image. The measured signal and the intensity of radiation were proportional to each other as shown in Eq. 2.2.

$$S_a = n_a (2\pi h c^2 \tau_a) \int_{\lambda_{a1}}^{\lambda_{a2}} \frac{\varepsilon(\lambda) f(\lambda)}{\lambda^5 (e^{hc/\lambda kT} - 1)} d\lambda \quad (2.2)$$

The total intensity of the blackbody radiation is obtained by integrating the right hand side of Eq. 2.2 over the radiation spectrum given by the filter wavelength in Fig 2.8. The measured signal and the total intensity of the blackbody radiation are plotted and fitted as seen in Figs. 2.18, 2.19 and 2.20 Using the result shown in these figures, three expressions were obtained from the ratio between the measured signals, one for each pair combination for the 3 filter wavelengths.

As seen in Figs. 2.18, 2.19 and 2.20 the relationship between the grayscale from the images and the intensity of radiation is found. It shows a linear relationship that can be used later to find the soot temperature. Each symbol in Figs. 2.18, 2.19 and 2.20 represents a different value of temperature; the temperature increment was about 25 °C. On the y axis for this curve the grayscale is divided by the shutter time to avoid saturation from the linear response. Once an image was taken, it was verified that no color was saturated anywhere in the image. The shutter time is increased to the point where no more saturation can be obtained. There is a great difference between the limit of saturation between two given wavelengths. For instance, at 1000 °C using the 550 nm filter wavelength, the shutter time is about 1/250 s. Whereas, for a 900 nm filter wavelength, the shutter time was about 1/3000 s. Thus, the shutter time has to be included in the calculation to avoid the limit of saturation in the images. On the x-axis, Eq. 2.2 is used to find the measured signal over the given temperature. The program found in Fig. 2.7 is also used with limits of integration given by the filter wavelength using a trapezoidal rule. Figures 2.18, 2.19 and 2.20 also show R^2 values, which are close to 1, indicating that the curve model closely fit the data. When using Spotlight to obtain the grayscale values, a uniform value of grayscale is seen over each pixel line drawn.

As seen on the left hand side of Figs. 2.17, the grayscale is almost constant. This is due to the fact that the blackbody cavity has a uniform temperature.



Figs. 2.17 Blackbody cavity image using a 550nm, 650 and 900nm Bandpass filter.

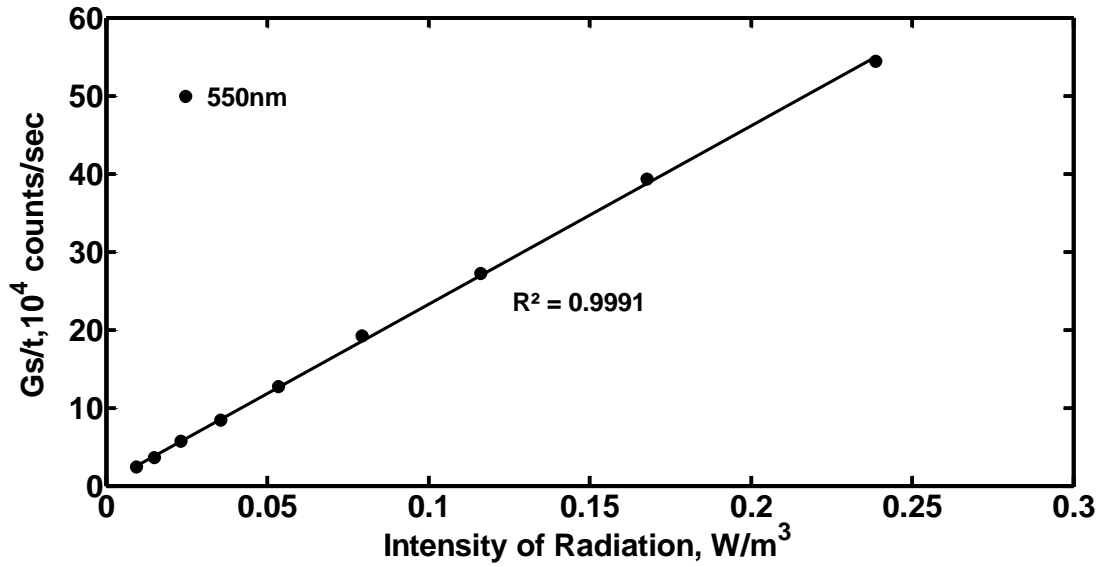


Fig. 2.18 Gray scale/shutter time versus light intensity using Plank's law for a camera and filter calibration for 550nm

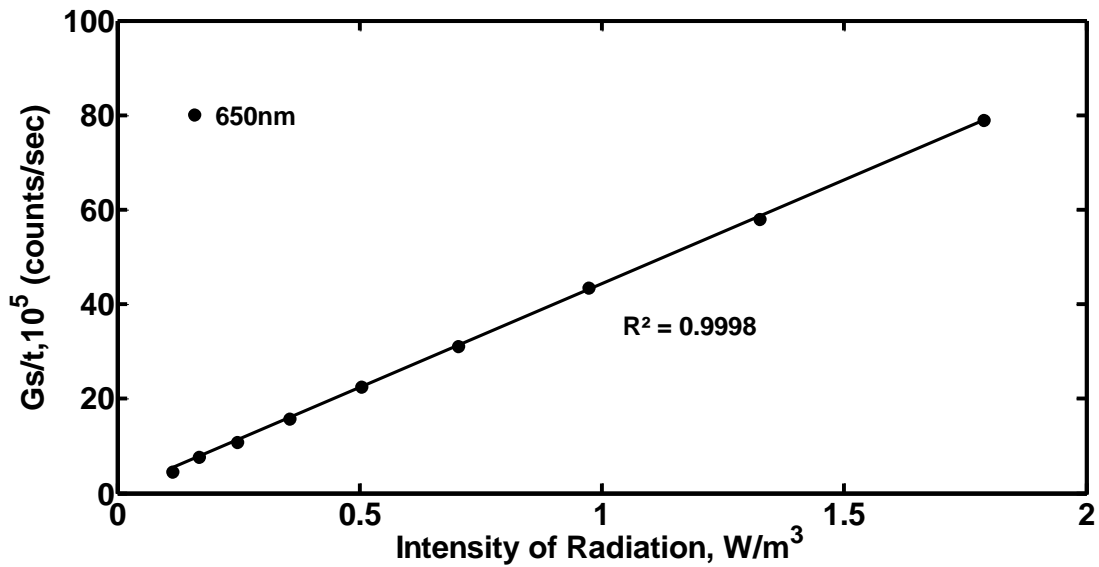


Fig. 2.19 Gray scale/shutter time versus light intensity using Plank's law for a camera and filter calibration for 650 nm

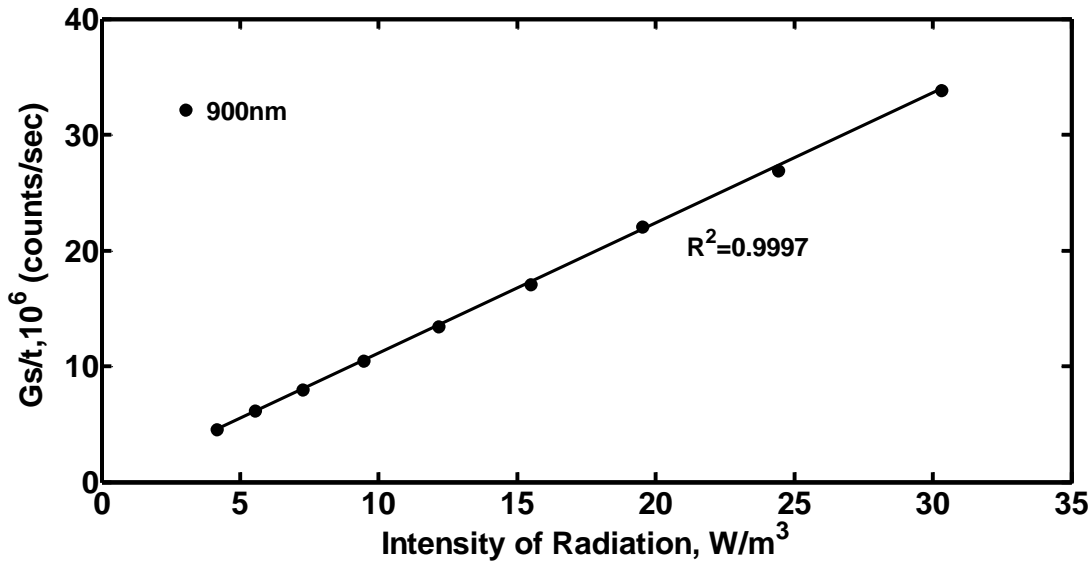


Fig. 2.20 Gray scale/shutter time versus light intensity using Plank's law for a camera and filter calibration for 900nm

For soot measurements, the emissivity ε is obtained from the result found by Chang and Charalampopoulos [28] where ε is proportional to $\lambda^{-1.38}$. The equation that directly relates the measured signal of any flame with the radiation emitted by soot particles is:

$$\frac{\frac{S_{\lambda_a}}{\tau_a}}{\frac{S_{\lambda_b}}{\tau_b}} = n_{ab} \frac{\int_{\lambda_{a1}}^{\lambda_{a2}} \frac{\varepsilon(\lambda) f_a(\lambda)}{\lambda^5 (e^{hc/\lambda kT} - 1)} d\lambda}{\int_{\lambda_{b1}}^{\lambda_{b2}} \frac{\varepsilon(\lambda) f_b(\lambda)}{\lambda^5 (e^{hc/\lambda kT} - 1)} d\lambda} \quad (2.3)$$

This equation is a relationship found using two different wavelengths and Eq. 2.2 where the constants cancel out. The shutter time is included in this equation.

Using the blackbody calibration results found in Figs. 2.18, 2.19 and 2.20 each of the following relationships are found:

$$\frac{\frac{S_{650}}{\tau_{650}}}{\frac{S_{900}}{\tau_{900}}} = 3.966 \frac{\int_{640}^{660} \frac{\varepsilon(\lambda) f_{650}(\lambda)}{\lambda^5 (e^{hc/\lambda kT} - 1)} d\lambda}{\int_{890}^{910} \frac{\varepsilon(\lambda) f_{900}(\lambda)}{\lambda^5 (e^{hc/\lambda kT} - 1)} d\lambda} \quad (2.3a)$$

$$\frac{\frac{S_{550}}{\tau_{550}}}{\frac{S_{900}}{\tau_{900}}} = 2.086 \frac{\int_{540}^{560} \frac{\varepsilon(\lambda) f_{550}(\lambda)}{\lambda^5 (e^{hc/\lambda kT} - 1)} d\lambda}{\int_{890}^{910} \frac{\varepsilon(\lambda) f_{900}(\lambda)}{\lambda^5 (e^{hc/\lambda kT} - 1)} d\lambda} \quad (2.3b)$$

$$\frac{\frac{S_{550}}{\tau_{550}}}{\frac{S_{650}}{\tau_{650}}} = 0.523 \frac{\int_{540}^{560} \frac{\varepsilon(\lambda) f_{550}(\lambda)}{\lambda^5 (e^{hc/\lambda kT} - 1)} d\lambda}{\int_{640}^{660} \frac{\varepsilon(\lambda) f_{650}(\lambda)}{\lambda^5 (e^{hc/\lambda kT} - 1)} d\lambda} \quad (2.3c)$$

Equation 2.3a, 2.3b and 2.3c provide the ratio of the filter function wavelengths $f(\lambda)$ of each pair-wise filter combination, only taking into consideration the measured signals given by Eq. 2.2 to obtain values of temperatures. In this equation n_{ab} is found by the blackbody calibration, and the limits of integration are given by the filter transmittances. Using a ratio relationship provides an easy way to calculate the soot temperature of a flame without having to deal with the actual signal ratio itself. The signal ratio is given by Spotlight as a value of deconvolved intensity from 0 to 1. It is not possible to obtain a value of gray scale out of the

flame image using deconvolution. Therefore, the pyrometry method only takes into consideration the ratio between two wavelengths providing values of temperatures.

Equations 2.3 a, 2.3b, and 2.3c are plotted in Fig. 2.21. The temperature varies from 1200-2200 K. It is now possible to use equations 2.3a, 2.3b and 2.3c or to use Fig. 2.21 to find the soot temperature given its signal ratio.

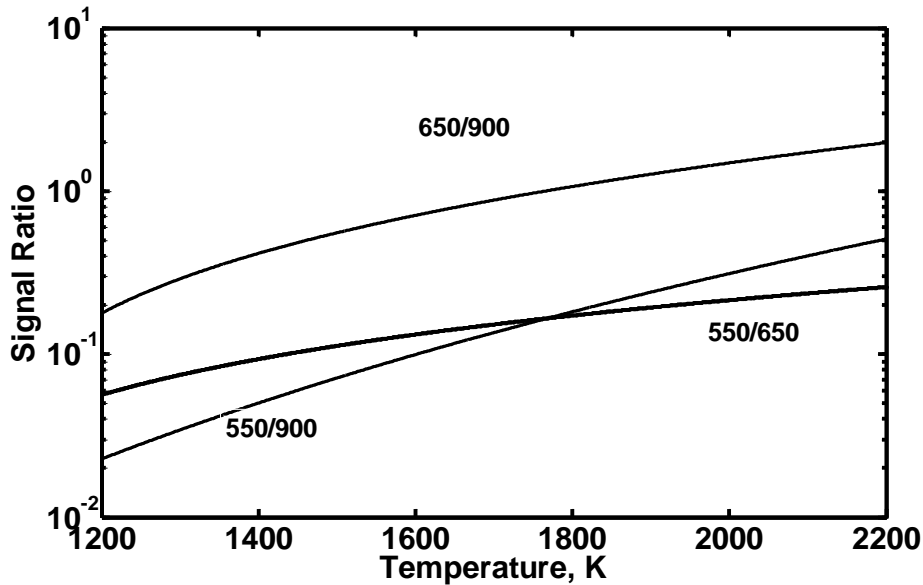


Fig. 2.21 Signal ratio vs. Soot Temperature for each pair wise combination filters

To obtain the uncertainty of the measurements in an axisymmetric flame using different wavelengths, it is necessary to find an expression that explains the relationship between the temperatures as a function of wavelength. If Eq. 2.3 is used, but rather than using the filter limit of integration given by the Fig 2.8, Fig 2.9, and Fig 2.10, a single value is chosen:

$$\frac{\frac{S_{\lambda_a}}{\tau_a}}{\frac{S_{\lambda_b}}{\tau_b}} = n_{ab} \frac{\frac{\varepsilon(\lambda_a) f_a}{\lambda^5 (e^{hc/\lambda kT} - 1)} \Delta\lambda_a}{\frac{\varepsilon(\lambda_b) f_b}{\lambda^5 (e^{hc/\lambda kT} - 1)} \Delta\lambda_b} \quad \text{Eq. 2.4}$$

$$\frac{\frac{S_{\lambda_a}}{\tau_a}}{\frac{S_{\lambda_b}}{\tau_b}} = C_{\lambda_a \lambda_b} \frac{\frac{\varepsilon(\lambda_a)}{(e^{hc/\lambda kT} - 1)}}{\frac{\varepsilon(\lambda_b)}{(e^{hc/\lambda kT} - 1)}} \quad \text{where} \quad C_{\lambda_a \lambda_b} = n_{ab} \frac{(f_a) \Delta\lambda_a (\lambda^5)_b}{(f_b) \Delta\lambda_b (\lambda^5)_a}$$

Re-arranging and solving for T an expression as a function of wavelength is found. Note that the emissivity varies as a function of wavelengths as explained previously. Therefore, the temperature is only dependent on the filter wavelengths and the signal ratio.

$$T = \frac{\frac{hc}{k} \left(\frac{1}{\lambda_b} - \frac{1}{\lambda_a} \right)}{\ln \left[\frac{1}{C_{\lambda_a \lambda_b}} \frac{(S_a / \tau_a) \varepsilon_{\lambda_a}}{(S_b / \tau_b) \varepsilon_{\lambda_b}} \frac{1 - \exp(-hc / k\lambda_a T)}{1 - \exp(-hc / k\lambda_b T)} \right]} \quad \text{Eq. 2.4 (a)}$$

In the expression $1 - \exp(-hc / k\lambda_a T)$ the exponential term is very small and can be drop from the equation without affecting the final value of soot temperature:

$$T = \frac{\frac{hc}{k} \left(\frac{1}{\lambda_b} - \frac{1}{\lambda_a} \right)}{\ln \left[\frac{1}{C_{\lambda_a \lambda_b}} \frac{(S_a / \tau_a)}{(S_b / \tau_b)} \left(\frac{\lambda_a}{\lambda_b} \right)^{1.38} \right]} \quad \text{Eq. 2.4 (b)}$$

Equation 2.4 b is a simplified version of equation of Eq. 2.3 where C is easily calculated using the calibration results found in Figs. 2.18, 2.19 and 2.20. Three dimensionless values were obtained; each one of them represented a pair-wise filter combination:

$$C_{\lambda_{550}\lambda_{650}} = 1.39; \quad C_{\lambda_{550}\lambda_{900}} = 28.38; \quad C_{\lambda_{650}\lambda_{900}} = 20.46$$

Using these calibration constants in Eq. 2.4 (b) and plotting them over a broad range of signal ratios, it was found that Eq. 2.4 followed a very similar curve as seen in Fig. 2.21 with a $\pm 10\text{K}$ temperature difference. This difference is due to the approximation in the filter curves. Because each band-pass filter possesses the same absolute error of ± 10 , mathematically, the uncertainty in the term $(\frac{1}{\lambda_b} - \frac{1}{\lambda_a})$ becomes smaller as the difference between λ_b and λ_a increases. Because the temperature in Fig. 2.4b is proportional to the term $(\frac{1}{\lambda_b} - \frac{1}{\lambda_a})$, larger differences between band-pass filter wavelengths will produce smaller uncertainties in temperature. Therefore, the idea of having the wavelength far away from each other reduces the uncertainty in the measurements.

Soot temperature measurements were carried out at nine different flame heights. For the temperature measurements, the average of the three temperatures using the specified wavelengths was obtained. As seen in Fig. 2.22 three flame images were taken each with a different filter. The importance of this method is that it is only necessary to take three images to have a complete temperature profile at any given height of an axisymmetric, optically thin flame. Measurements using other methods such as thermocouples require considerably more time beyond the one presented here.

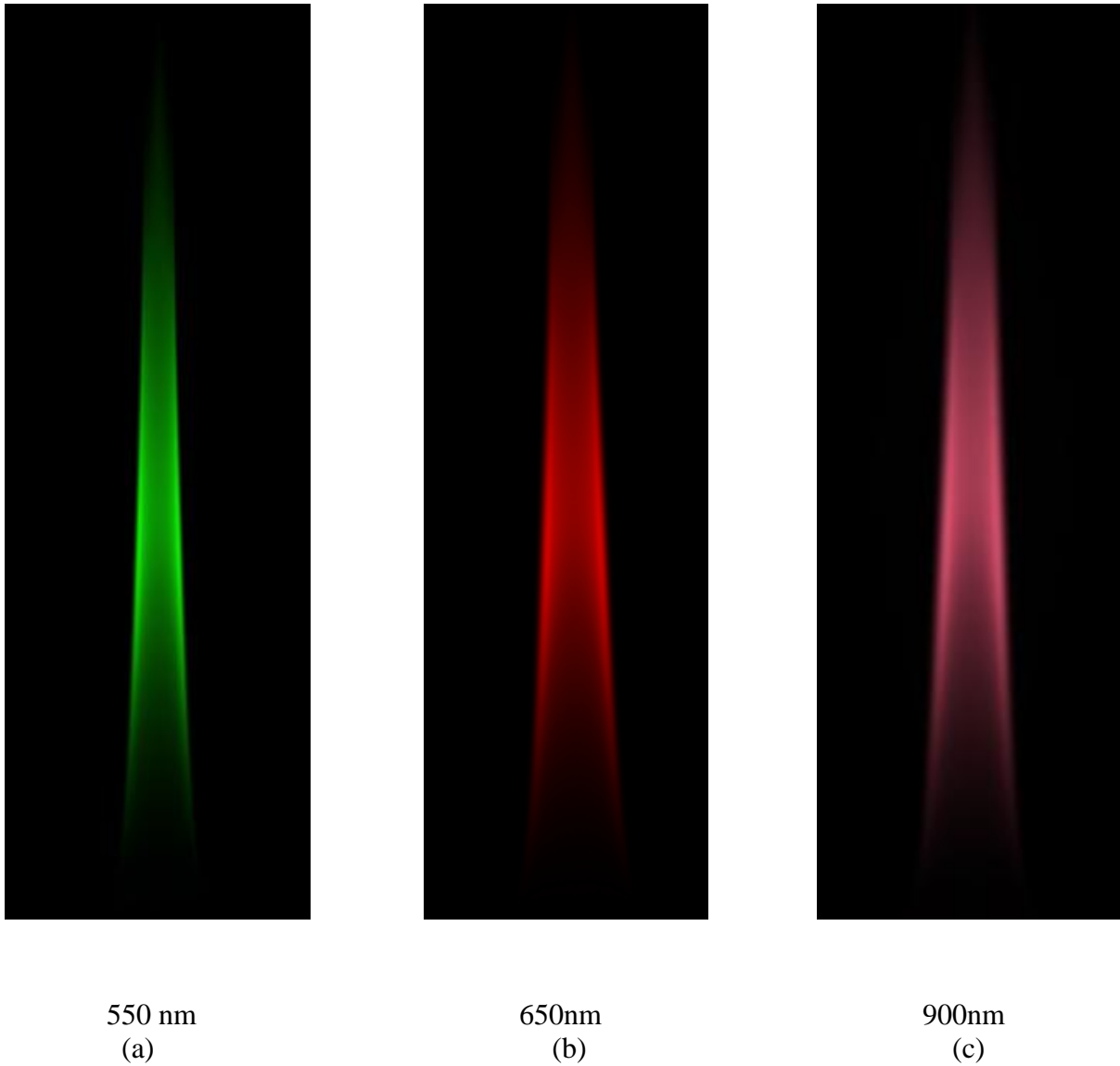


Fig. 2.22 flame images using three band-pass filters

Once three images were taken, the centerline was compared between them to make sure the images were at the same radial position. As seen in Fig. 2.26, the devolve intensity was given by the Abel transform tool where it provided values between 0 and 1 for each radial position in the flame. The line length pixel was converted to a radial value as shown in Fig. 2.23.

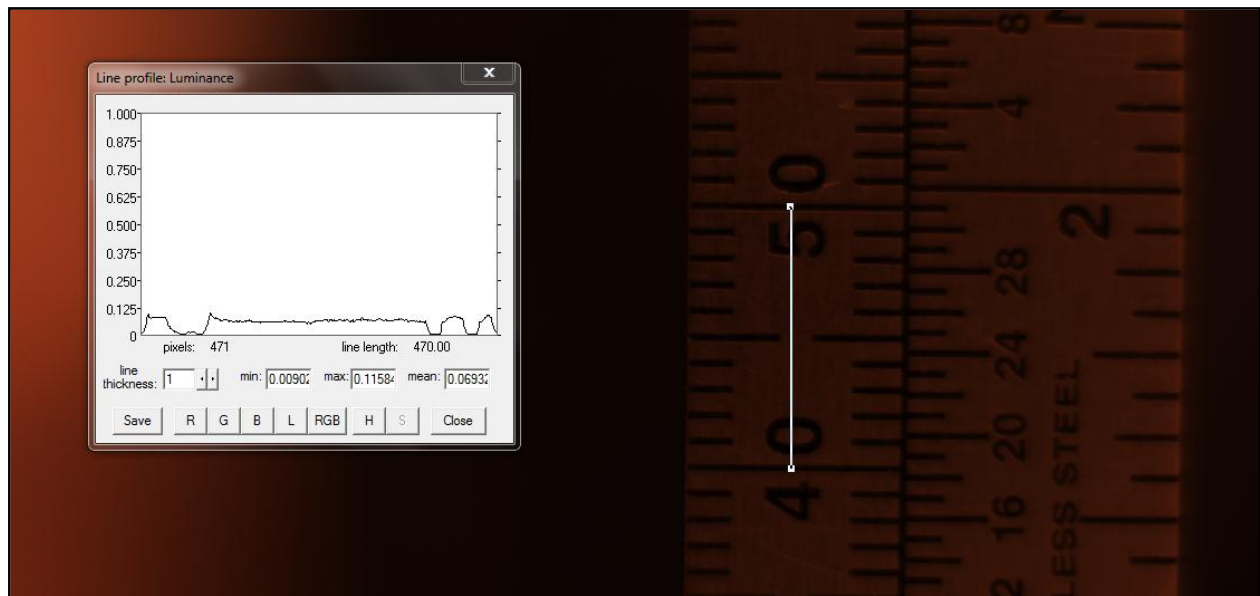


Fig. 2.23 Relationship between the grayscale and size of the flame.

The output from Spotlight 16 were arrays of x , y , R , G , B values. The x and y pixel coordinates were converted to a height above the burner and a radius where the origin is the center of the fuel port. It is necessary to find a relationship between the actual size of the flame and the line profile used. As seen in Fig. 2.23 a ruler was set in front of the camera from the tip of the burner. It can also be seen that the line length used, 470 pixels, represents about 10 mm. This calibration was later used to convert pixels to radial distance from the burner. The importance of the radial distance is to find the temperature at a given point in the flame. The line profile only takes into consideration the pixel length vs. the actual length. After finding the right value of calibration, an image of an object of known length was taken to validate that the value found in the calibration works with any type of image.

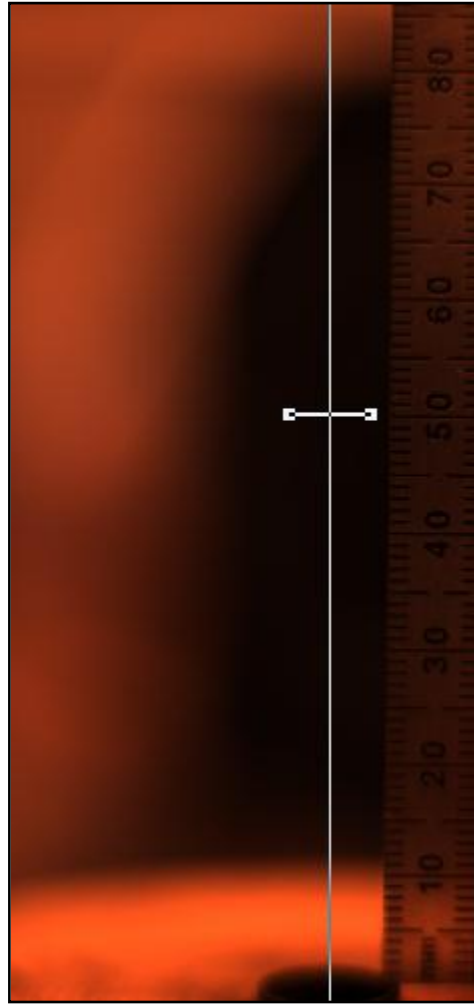


Fig. 2.24 Ruler used to find the position of the flame height.

The height of the flame at which the temperature is taken was found using Fig. 2.24. The image was opened using Spotlight, and the Abel tool is set at the needed height. The flame image is then opened, and the analysis is performed. The Spotlight program uses the Abel transform given by Eq. 2.5 [25]:

$$F(r) = -\frac{1}{\pi} \int_r^{\infty} \frac{p(l)}{\sqrt{l^2 - r^2}} dl \quad \text{Eq. 2.5}$$

A filtered Abel transform was selected, which incorporates a data filtering operation. Various filtering schemes are provided as seen in Fig. 2.25.

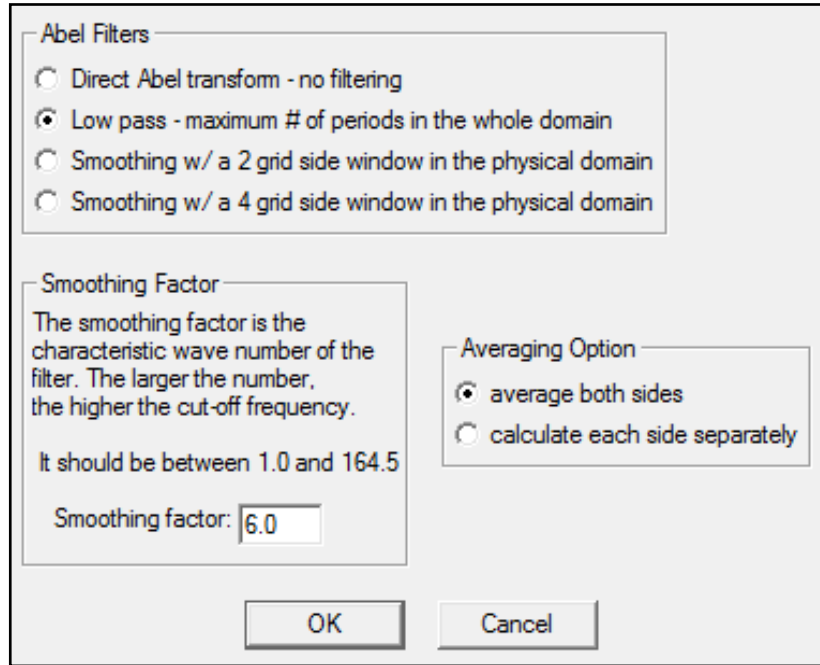


Fig. 2.25 Abel filters options in Spotlight.

The Abel transform tool consists of a horizontal line profile and a vertical centerline. It is assumed that the flame orientation is vertical such that the horizontal profile cuts perfectly across it. If an image must be rotated, the angle tool may be used for this purpose. If a reference image is used, it must be rotated in exactly the same way as the flame image. The tool's vertical centerline is positioned in the center of the flame with the horizontal profile line positioned at the desired height along the flame. This will provide the deconvolved intensity as seen in Fig. 2.26. As the tool is moved, the line profile is displayed "live" in the dialog box. The distribution is plotted (red) in the window along with flame profile (black) and reference profile (blue). The

centerline (green) is included to help with visualization. The profile length is forced to be symmetric.

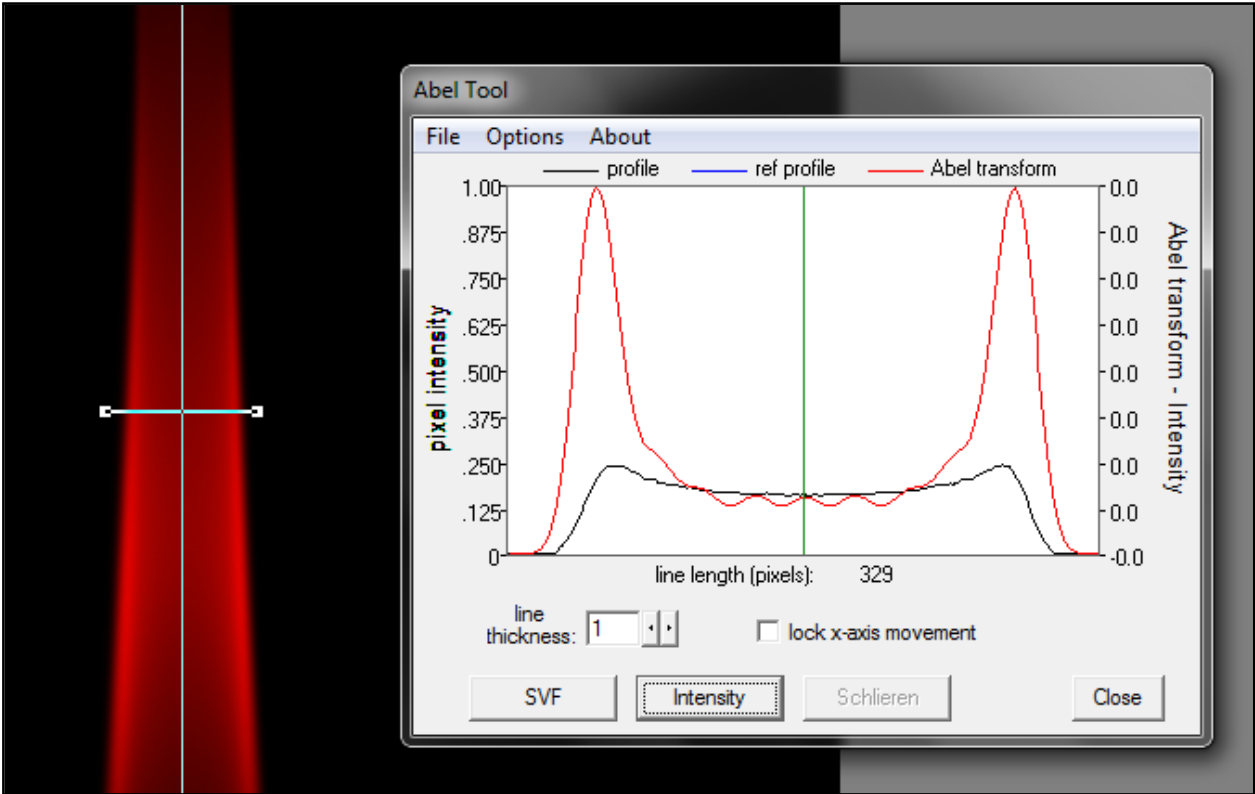


Fig. 2.26 Abel deconvolved intensity for a 650 nm wavelength.

Another advantage of using a ratio pyrometry to find the value of temperatures is that the Abel deconvolved intensity can be used as given by Spotlight, which is a value from 0 to 1. Otherwise, it would have been necessary to convert to grayscale, a much more difficult calculation. Since a pair-wise combination is used, the soot temperature can be obtained in a straight forward way using the calibration equation and the signal ratio.

Chapter 3: Results and Discussion

Present measurements of deconvolved intensities of radial distributions ranging from 0 to 6 mm at various flame heights are shown in Figs. 3.1, 3.2 and 3.3. The deconvolved intensities were obtained from the spectral radiation intensities of the flame images. Because the flame was optically thin, the spectral radiation intensity measurements could be properly deconvoluted using Spotlight to provide the radial distributions of soot temperatures.

The deconvolved intensities in Figs. 3.1, 3.2 and 3.3 were only found at radial distance from 3.5 to 6 mm. The deconvolved profiles were not provided in the region between 0 and 3.5 mm due to the absence of soot radiation. In this region deconvolution errors lead to large uncertainties. It is important to note that the centerlines of the deconvolved profiles have to be placed in the same radial position in order to compare their signal ratios. In all deconvolved images symmetry was forced.

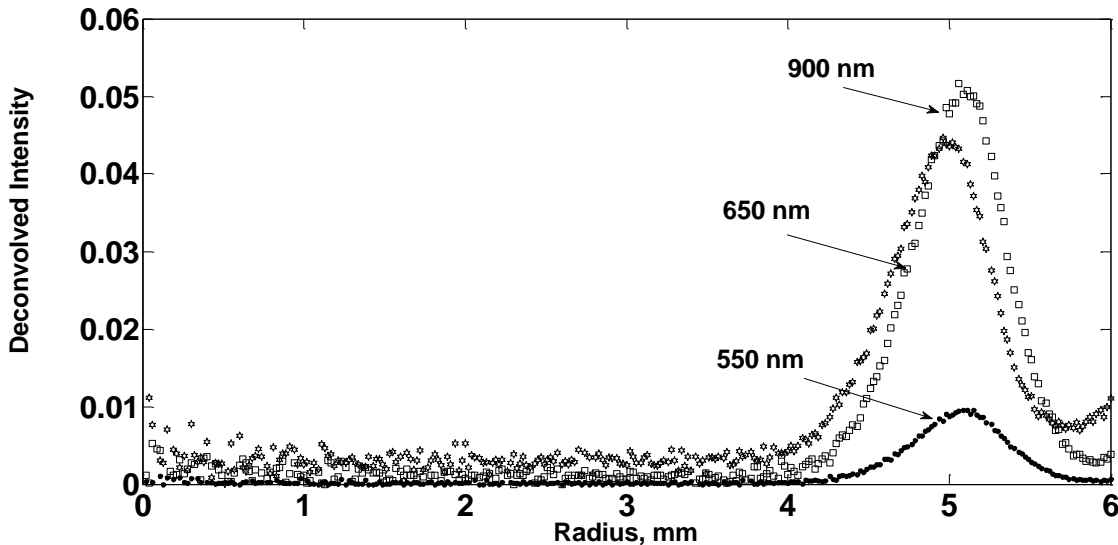


Fig 3.1. Deconvolved intensity vs. radius at 7 mm flame height.

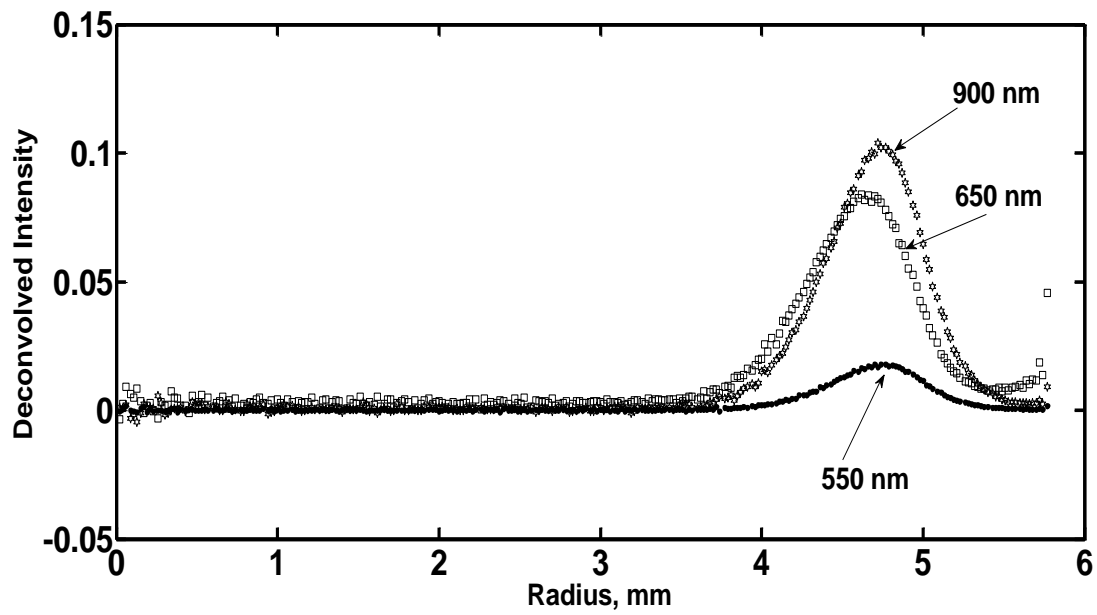


Fig 3.2. Deconvolved intensity vs. radius at 10 mm flame height.

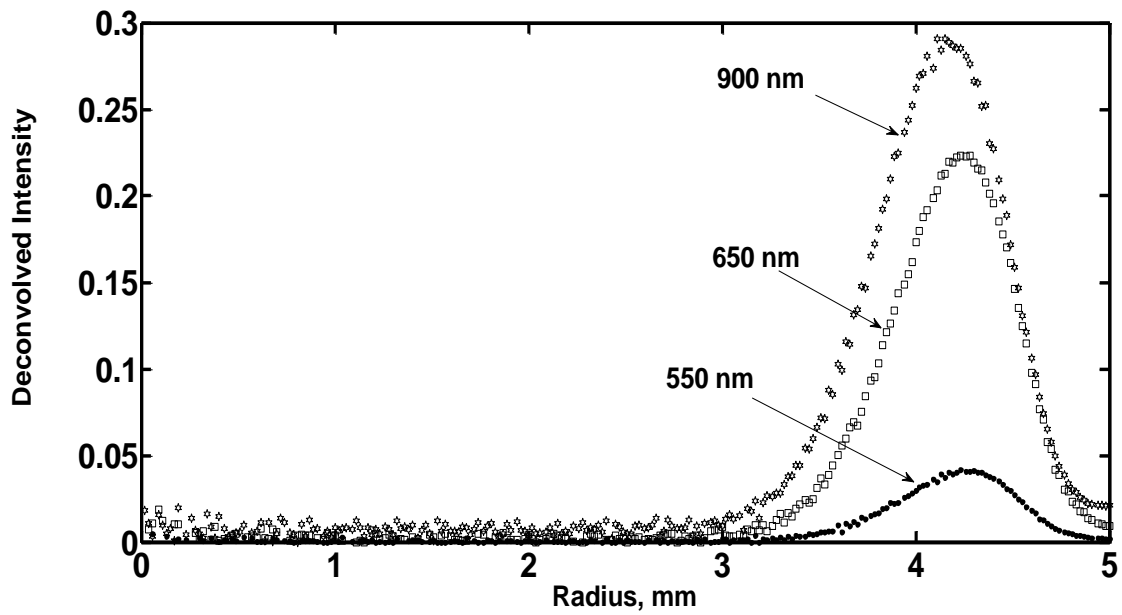


Fig 3.3. Deconvolved intensity vs. radius at 15 mm flame height.

Comparing the deconvolved intensities at radial distance from 3 to 5 mm in Figs. 3.1, 3.2, 3.3, 3.4 and 3.5 it is found that the deconvolved profiles have peak intensities at large radial distances from the centerline of the flame. Peak intensity occurs at a radial distance of approximately 4.5 mm for 7, 10 and 15 mm heights and at approximately 3.7 mm for a 20 mm height. At radial distances between 0 and 3 mm these peaks does not exist mainly due to the fact that soot radiation intensities decreases to zero near the flame centerline.

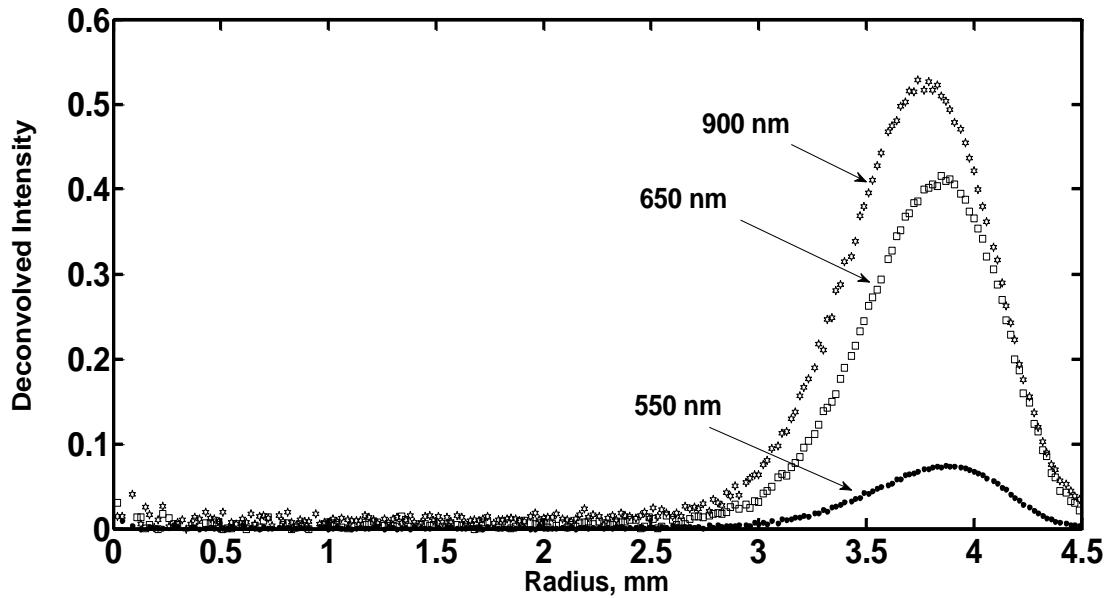


Fig 3.4. Deconvolved intensity vs. radius at 20 mm flame height.

For Fig. 3.5 and 3.6 deconvolved intensities are available at radial distances from 0 to approximately 3 mm. The radiation signal strength decreases at the outer part of the flame after 3 mm radius. The peak intensities occur at 2.5 mm for a 50 mm flame height. However, for a 70 mm flame height, the peak intensity occurs at the centerline of the flame as seen in Fig. 3.6.

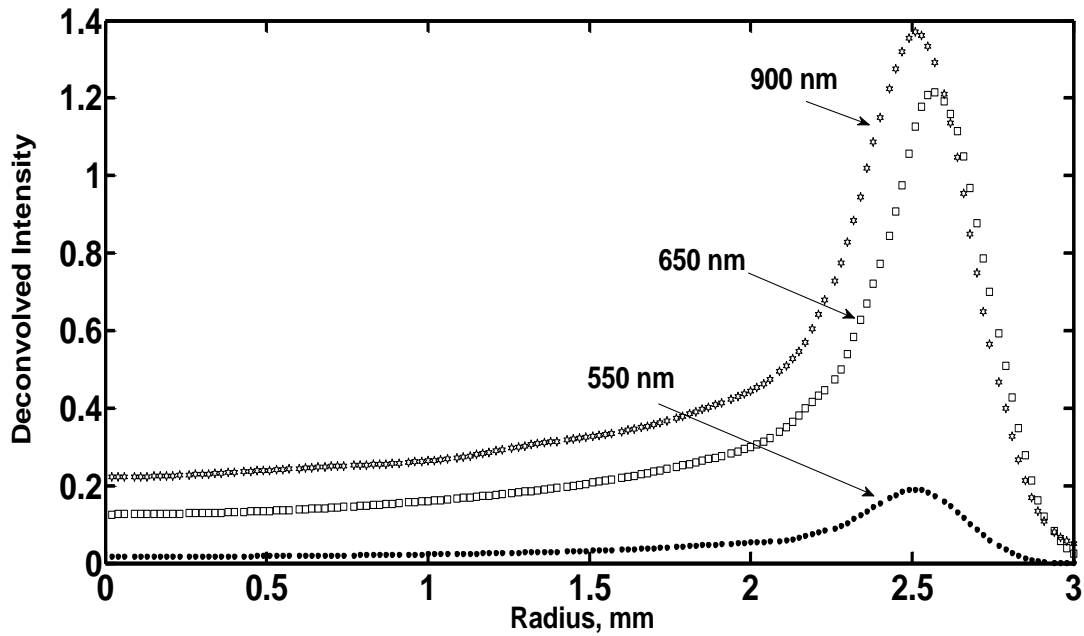


Fig 3.5. Deconvolved intensity vs. radius at 50 mm flame height.

The deconvolution measurements above the 70 mm height were problematic due to flickering of the flame tip; it was almost impossible to obtain a steady measurement in this region. Measurements were stopped at a height of 70 mm height even though the total flame height was about 88 mm.

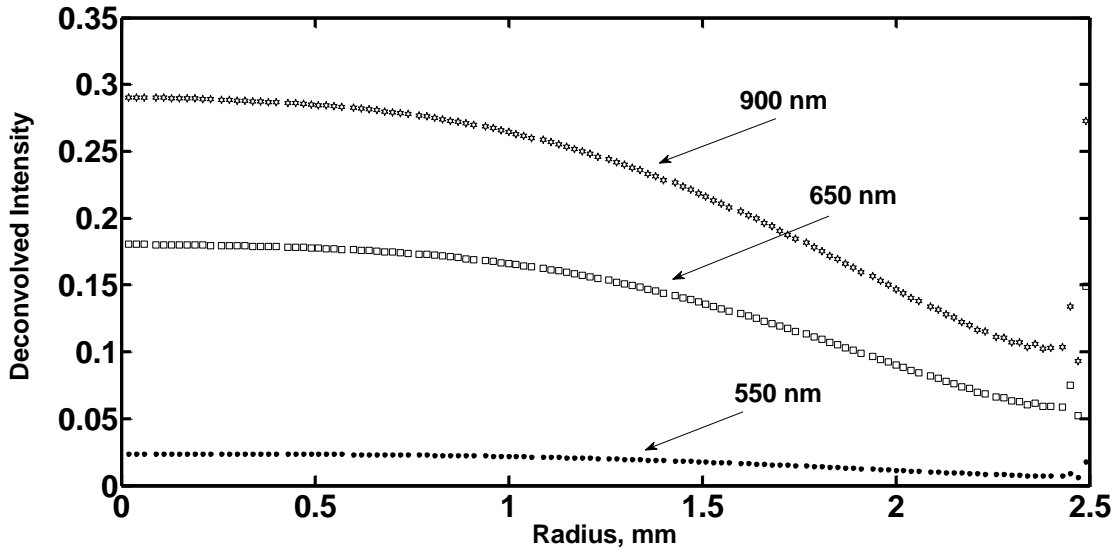


Fig 3.6. Deconvolved intensity vs. radius at 70 mm flame height.

The measured temperature is in good agreement with the published results as seen in Fig. 3.7 [4,5]. The soot temperature profile found here is similar to the one found using thermocouples. It was possible to obtain the temperature throughout the whole range of radial distance and at any given flame height from the top of the burner. The only condition is that the soot has emissivity high enough to supply radiation coming from the flame sufficient to provide deconvolved values that can be transformed to temperature.

In addition, there was difficulty in obtaining temperatures at the edges of the flames and at heights above 70 mm. In these regions, the data scattered. Even though the flame was axisymmetric, there was still some flickering at the tip of the flame therefore; the deconvolved signal has random behavior making it difficult to obtain temperatures values.

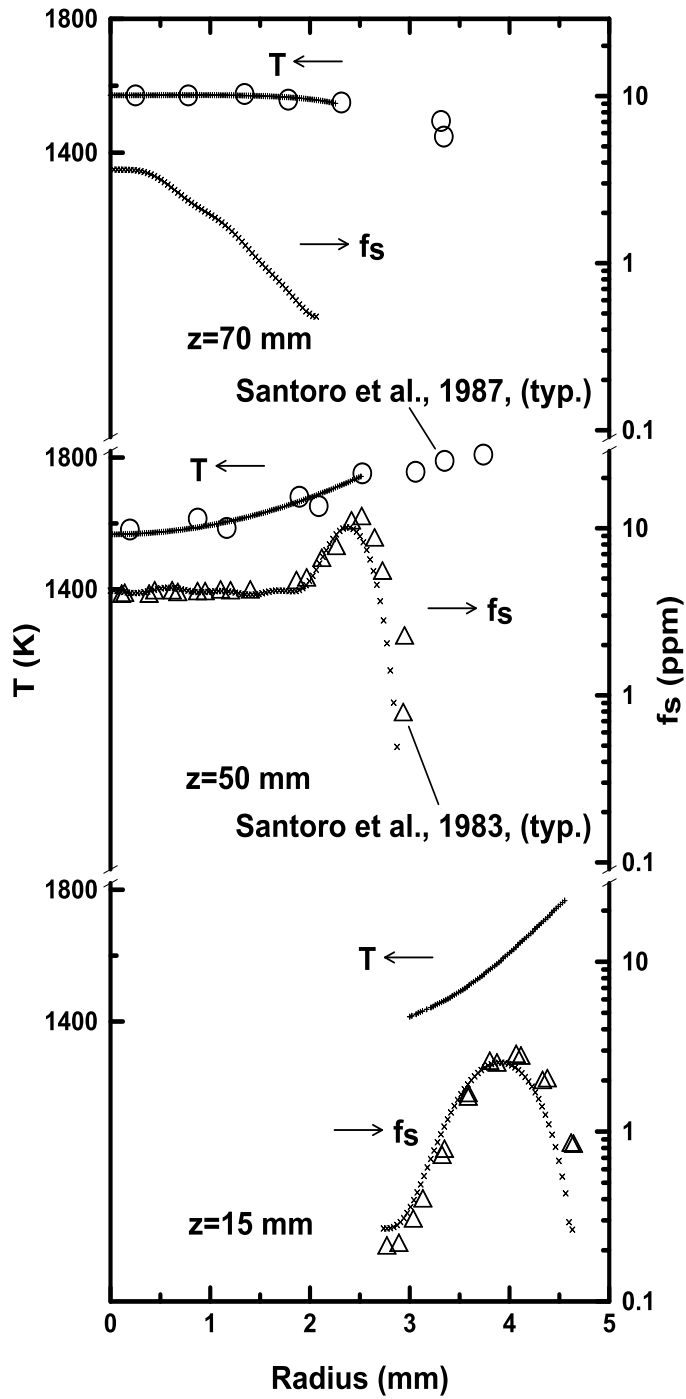


Fig. 3.7 Measured temperature at three flame heights (15, 50 and 70 mm) above the burner and compared with soot volume fraction from Santoro's paper [4,5,31].

The radial distance from the flame center, where soot temperature measurements begin to lose precision, is seen in Fig. 3.8. In this figure the data start scattering at a radial distance of more than 3 m. Therefore, no temperature profile is shown after this value. In this region the measurements are close to the limit of saturation where the soot concentration decreases below 0.1 ppm as seen in Fig 3.7 for a 50 and 70 mm height. For this reason, just a portion of the flame temperature was obtained in this range. It can be seen in Figs. 3.8 and 3.9 that soot concentrations are high enough, over a range of temperature $1250\text{ K} < T < 2000\text{ K}$, to provide good temperature values. It is important to point out that past studies that measured flame temperatures with thermocouples, found similar results as here where temperatures peak at radial distances beyond where soot is at its highest concentrations [4,5,30]. This is due to the fact that thermocouples are not restricted to the amount of soot in a flame. Therefore, they can even be used in a region outside the flame.

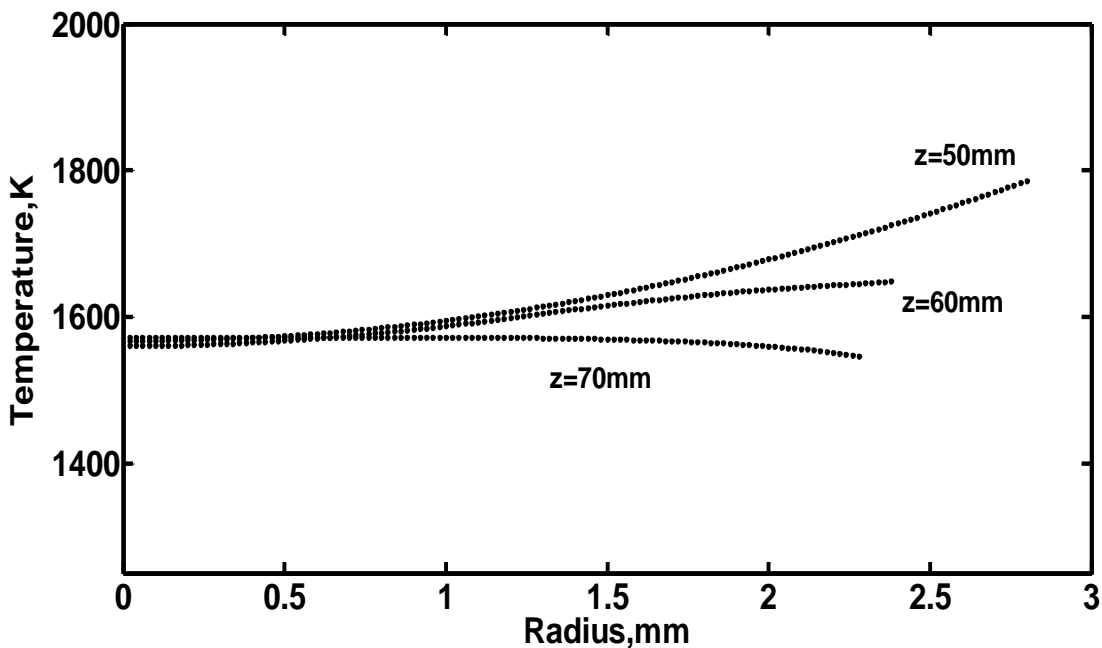


Fig. 3.8 Measured temperatures at three heights above the coflow burner.

Insufficient soot concentration also affects the overall temperature profile measured at axial locations between the burner and the flame tip. As a result, soot temperatures can only be accurately measured for soot volume fractions above 0.1 ppm. At a height of 15 mm, flame temperatures can only be measured for soot concentrations ranging from 0.2 to 3 ppm. Whereas at a height of 70 mm, flame temperatures can only be measured for soot concentrations ranging from 0.4 to 4 ppm as seen in Fig. 3.7. The deconvolved intensity is shown in Figs. 3.1 thru 3.6. It is important to note that after the images are deconvolved and transformed into temperature, the three temperature profiles are averaged without applying any filter to remove noise. This is done because the data has already been filtered by the Abel transform as shown in Fig. 2.25. Therefore, the graphics followed a smooth behavior making it unnecessary to apply any other filtering.

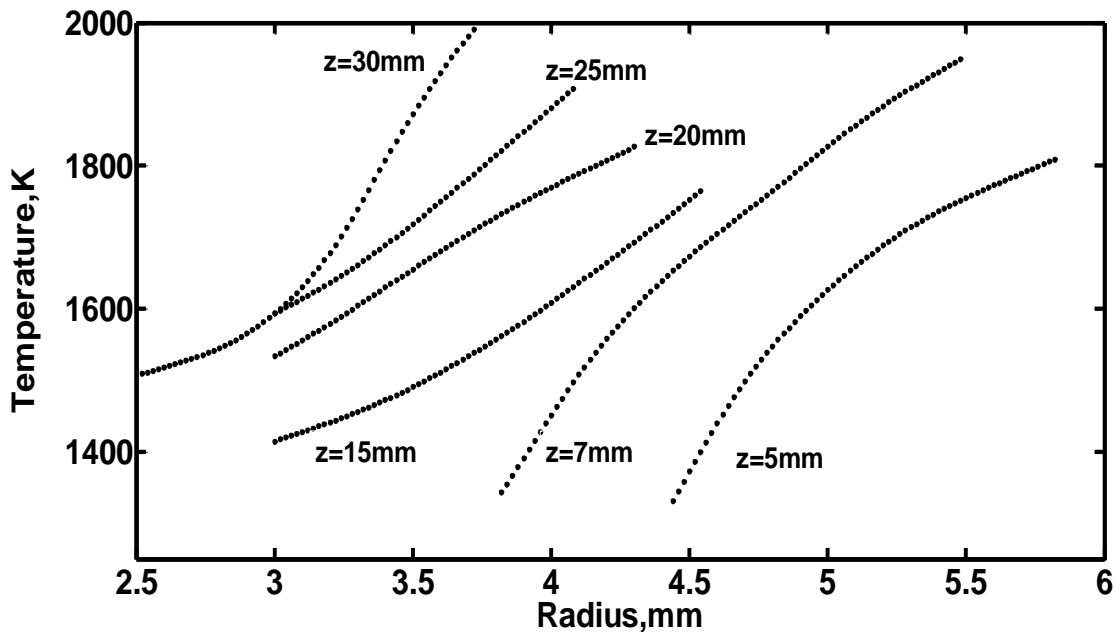


Fig. 3.9 Measured temperatures at six heights above the coflow burner.

Figures 3.8 and 3.9 only show half of the temperature profile. This is due to the fact that the flame is assumed axisymmetric. In Figure 3.9 the temperature profile moves toward the left as it moves up from the flame bottom. From a radial distance of 0-3 mm from the center of the burner, there are no temperature responses for flame heights from 0-50 mm. However, when a height of 50 mm is reached as seen in Fig. 3.8, it is possible to measure the soot temperature in the radial distance of 0-3 mm. The amount of emissivity found in the regions where the images are taken is directly related to the accuracy of the results.

Chapter 4: Conclusions

Flame structure and soot processes were studied for various soot paths in ethylene/air laminar coflowing jet diffusion flames to supplement recent measurements limited to the axis of ethylene/air laminar jet diffusion flames. The major conclusions of the study are as follows:

1. Soot temperature was measured in a laminar axisymmetric flame with a modified digital camera. This low-cost consumer color digital camera for full-field soot temperature measurements provides a fast and convenient way to measure soot temperature with high resolution and accuracy in axisymmetric and optically thin flames. The method to calculate the soot temperature developed in this paper can be used affordably in other laboratories making it possible to reproduce and obtain similar results. For the highest accuracy, full calibrations like the one herein will be required. Guidance is provided here for future investigators interested in calibration using a digital camera.
2. Deconvolved intensities are available only in flame regions possessing both sufficient soot temperatures and soot volume fractions. Temperatures in the range of 1250 to 2000 K as well as soot volume fractions greater than 0.1 ppm are required to achieve usable deconvolved intensities. These conditions are met for flame heights above 50 mm near the flame centerline between 0 and 3 mm and for flame heights

below 30 mm in the outer radial boundary of the flame between 3 and 6 mm. The results were compared with past works and reasonable agreement was observed

References

- [1] An Introduction to Combustion Concepts and Applications, Stephen R. Turns, McGraw Hill, 2nd edition. p. 305-362.
- [2] K. Smyth, J. Houston, R. Dorfman, R. Santoro, Soot Inception in a Methane/ air diffusion flame. *Combust. And Flame* 62:157-181 (1985).
- [3] Siegel, Robert; Howell, John R. (2002). *Thermal Radiation Heat Transfer; Volume 1* (4th ed.). Taylor & Francis. p. 1-31.
- [4] R.J. Santoro, H.G. Semerjian, and R.A. Dobbins, *Combustion and Flame* 51 (1983), 203-218.
- [5] R. J. Santoro, T. T. Yeh, J. J. Horvath, and H. G. Semerjian, "The transport and growth of soot particles in laminar diffusion flames," *Combustion Science and Technology* 53, 89-115 (1987).

- [6] H. I.Joo, O. L. Gulder, "Soot formation and temperature field structure in co-flow laminar methane-air diffusion flames at pressures from 10 to 60 atm," *Proceedings of the Combustion Institute* 32, 769-775 (2009).
- [7] R. Lemaire, P. Desgroux, "Experimental comparison of soot formation in turbulent flames of Diesel and surrogate Diesel fuels," *Proceedings of the Combustion Institute* 32, 737-744 (2009).
- [8] S. D. Iuliis, G. Zizak, "2D soot volume fraction imaging in an ethylene diffusion flame by two-color laser-induced incandescence (2C-LII) technique and comparison with results from other optical diagnostics," *Proceedings of the Combustion Institute* 31, 869-876 (2007).
- [9] S. D. Iuliis, M. Barbini, S. Benecchi, F. Cignoli, and G. Zizak, "Determination of the soot volume fraction in an ethylene diffusion flame by multiwavelength analysis of soot radiation," *Combustion and Flame* 115, 253-261 (1998).
- [10] F. Cignoli, S. D. Iuliis, V. Manta, and G. Zizak, "Two-dimensional two-wavelength emission technique for soot diagnostics," *Applied Optics*. Vol. 40, No. 30, (2001).

- [11] P. B. Kuhn, B. Ma, B. C. Connelly, M. D. Smooke, M. B. Long, "Soot and thin-filament pyrometry using a color digital camera," Proceedings of the Combustion Institute (2010).
- [12] Snelling, D.R., Thomson, K.A., Smallwood, G.j., Gulder, O.L., Wecman, E.J., and Fraser, R.a., AIAA Journal 40: 1789-1795 (2002).
- [13] Lenvendis, Y.A., Estrada, R.E., and Hottel, H.C., Review of Scientific Instruments 63: 3608-3622(1992).
- [14] Lee, W., and Na, Y.D., Soot Study in Laminar Diffusion Flames using Two-color Pyrometry and Abel Inversion, 4th JSME-KSME Thermal Engineering Conference, Kobe, Japan, (2000).
- [15] Panagiotou, T., Levendis, Y., and Delichatsios, M., Measurements of particle flame temperatures using three-color optical pyrometry Combustion and Flame 104: 272-287 (1996).
- [16] Zhao, H., and Ladommantos, N., Optical diagnostic for soot temperature, Progress in Energy and Combustion Science 24: 221-225 (1998)

- [17] Bolough, M.B., and Ahrens, T.J., Review of Scientific Instruments 60: 3711-3716 (1989)
- [18] Anselmi-Tamburini, U., Campari, G., Spinolo, G., and Lupotto, P., Review of Scientific Instrumentation 66: 50006-50014 (1995)
- [19] B.B. Connelly, S.A. Kaiser, M.D. Smooke, and M.B. Long, Two-dimensional soot pyrometry with a color digital camera, Joint meeting of the U.S. Sections of the Combustion. Inst., Philadelphia, 2005.
- [20] P.B. Kuhn, B. Ma, B.C. Connelly, M.D. Smooke, and M.B. Long, Proceedings of the Combustion Institute. 33 (2011), 743-750.
- [21] S. di Stasio and P Massoli, Influence of the soot property uncertainties in temperature and volume-fraction measurements by two-color pyrometry, 1994 Meas. Sci. Technol. 5 1453
- [22] R. Klimek, T. Wright, "Spotlight: Image analysis and object tracking software," <http://microgravity.grc.nasa.gov/spotlight/>.

- [23] Wolfram Math world, Built with mathematics technology
<http://mathworld.wolfram.com/GaussianFunction.html>.
- [24] D. Coffin, “Decoding raw digital photos in Linux,”
<http://www.cybercom.net/~dcoffin/dcrawl/>.
- [25] Z. Yuan, The filtered Abel transform and its application in combustion diagnostics, Western Section of the Combustion Institute, Stanford, 1995.
- [26] MATLAB 6.1, The MathWorks Inc., Natick, MA, 2010
- [27] Newport filters curves, 550,650, 900 nm. Newport Corporation. Irvine, CA
92606
- [28] Nikon D700 spectral sensitivity,
http://www.maxmax.com/nikon_d700_study.htm.
- [29] H. Chang, T.T. Charalampopoulos, Determination of wavelength dependence of refractive indices of flame soot, Proceedings of the Royal Society of London Series A- Mathematical Physical and Engineering Sciences 430 (1990), 577-591.

- [30] C.S. Mcenally, M.D. Smooke, R.J. Hall, Computational and Experimental study of soot in a Coflow Laminar Ethylene Diffusion Flame, Combust. Inst., 1998/pp.1497-1505.
- [31] Jose A. Castillo, Haiqing Guo, Peter B. Sunderland, Measurement of Soot Temperature and Soot Volume Fraction in a Diffusion Flame using a digital camera, Spring Technical Meeting of the Central States Section for the Combustion Institute, Department of fire protection Engineering, University of Maryland, April 22-24, 2012.